https://doi.org/10.5194/egusphere-2026-3119
Preprint. Discussion started: 16 June 2026

Understanding ecosystem gross primary productivity, evapotranspiration, and water use efficiency of maize using ISBA-A-g_s land surface model over temperate and tropical semi-arid climates

Syam Chintala[1*], Lionel Jarlan[2], Vincent Rivalland[2], Aaron Boone[3], Oluwakemi Dare-Idowu[4,5], Valerie Le Dantec[2], Gilles Boulet[2,6], BVN P Kambhammettu[1] and Aurore Brut[2]

[1]Department of Civil Engineering, Indian Institute of Technology Hyderabad, Sangareddy, Telangana, India.

[2]CESBIO, Universite de Toulouse, CNES/CNRS/INRAE/IRD/UT, Toulouse, France.

[3]Centre National de Recherche's Meteorological (CNRM), Meteo-France/CNRS, Toulouse, France.

[4]Agricome Project Solutions Limited, Abuja, Nigeria.

[5]Lead City University, Ibadan, Nigeria.

[6]Indo-French Cell for Water Sciences, ICWaR, Indian Institute of Science, Bangalore, India.

*Corresponding author: Syam Chintala, E-mail: ce22resch11012@iith.ac.in, Tel: +91 7997014429

Abstract

Water use efficiency (WUE), a key ecohydrological indicator linking carbon assimilation and vegetation water loss, is critical for understanding ecosystem responses under changing hydro-climatic conditions. Process-based land surface models (LSMs) are widely used to represent carbon-water interactions; however, their ability to simulate ecosystem-scale WUE across contrasting climates remains limited. This study evaluates the performance of the Interactions between Soil-Biosphere-Atmosphere model with A-g_s photosynthesis scheme (ISBA-A-g_s) implemented within the SURFEX land surface modelling platform in simulating gross primary

https://doi.org/10.5194/egusphere-2026-3119
Preprint. Discussion started: 16 June 2026

productivity (GPP), evapotranspiration (ET), and WUE (GPP/ET) for maize grown under temperate (France, FR-Lam) and tropical semi-arid (India, Ind-IITH) climates. The model was driven by site-specific meteorological and vegetation variables across six growing seasons under sprinkler irrigation at FR-Lam, and two seasons (monsoon and winter) under alternate furrow irrigation (AFI) at Ind-IITH. Model calibration revealed that FR-Lam is characterized by relatively higher cuticular conductance and pronounced atmospheric control on stomatal behaviour, whereas at Ind-IITH, AFI-induced adjustments in mesophyll conductance and soil moisture stress thresholds. At FR-Lam, ISBA-A-g_s simulated the seasonal mean cumulative GPP, ET, and WUE of 1039 ± 20 gC m^{-2}, 610 ± 31 kg H_2O m^{-2}, and 1.70 ± 0.10 gC kg^{-1} H_2O, respectively, as compared to measured values of 1026 ± 30 gC m^{-2}, 562 ± 42 kg H_2O m^{-2}, and 1.82 ± 0.11 gC kg^{-1} H_2O correspondingly. At Ind-IITH, the model simulated the seasonal mean cumulative GPP, ET, and WUE of 766 ± 15 gC m^{-2}, 567 ± 30 kg H_2O m^{-2}, and 1.35 ± 0.11 gC kg^{-1} H_2O, respectively, as compared to measured values of 793 ± 11 gC m^{-2}, 522 ± 20 kg H_2O m^{-2}, and 1.51 ± 0.12 gC kg^{-1} H_2O correspondingly. Further, the diagnostic analysis using the GPP·$VPD^{0.5}$-ET relationship revealed that ISBA-A-g_s realistically captures the coupling between carbon assimilation and transpiration-driven water loss. Overall, ISBA-A-g_s demonstrates strong capability in simulating carbon and water fluxes of maize, particularly in representing WUE dynamics under contrasting climate regimes.

Keywords: Ecosystem modelling, Gross primary productivity, Evapotranspiration, Water use efficiency, Maize, Climate.

Research Highlights:

1. Multi-energy balance ISBA-A-g_s was applied to simulate maize WUE across temperate and tropical semi-arid climates.

https://doi.org/10.5194/egusphere-2026-3119
Preprint. Discussion started: 16 June 2026

2. Parameter calibration improved GPP simulations more substantially than ET.
3. The model reproduces irrigation-driven divergence in tropical semi-arid conditions, reflecting robust soil moisture stress and canopy resistance parameterization.
4. ISBA-A-g_s successfully reproduces the GPP·$VPD^{0.5}$-ET relationship, indicating a realistic representation of photosynthesis-transpiration coupling.

1.0 Introduction

Water use efficiency (WUE) is a key ecohydrological indicator that deals with carbon and water cycles in terrestrial ecosystems (Chen et al., 2022; Ito and Inatomi, 2012; Yu et al., 2008). By linking carbon assimilation (as a proxy for photosynthesis) with vegetation water loss (as a proxy of evapotranspiration), WUE provides an integrated measure of ecosystem functioning at the land-atmosphere interface (Beer et al., 2009; Xue et al., 2015). At the ecosystem scale, WUE is typically defined as the ratio of gross primary productivity (GPP) to evapotranspiration (ET) over a relatively homogeneous surface (Beer et al., 2009; Vadez et al., 2023). In essence, it quantifies how efficiently agro-ecosystems convert available water into biomass through photosynthesis, with higher WUE indicating greater carbon gain per unit of water consumed. Micrometeorological approaches, particularly the eddy covariance (EC) setups, are now widely used through international networks (FLUXNET, NEON, ICOS, AMERIFLUX) to directly measure surface-atmosphere exchanges of carbon and water fluxes at the ecosystem scale (Aubinet et al., 1999; Baldocchi, 2014; Baldocchi et al., 2001; Pastorello et al., 2020; Reichstein et al., 2005). Despite their robustness, EC measurements are constrained by limited spatial representativeness, high installation and maintenance costs, and sensitivity to surface heterogeneity (Hoover et al., 2023).

Maize (*Zea mays L.*) is one of the most widely cultivated cereal crops globally (15% of cultivated area) and serves as a staple food, feed, and bioenergy source, contributing

https://doi.org/10.5194/egusphere-2026-3119
Preprint. Discussion started: 16 June 2026

substantially to global food security (Erenstein et al., 2022; Tanumihardjo et al., 2020). Gross primary productivity of maize typically ranges between 1500-2000 gC m^{-2} per growing season, depending on climate, management, and cultivar, with higher values observed under well-managed, irrigated systems (Beer et al., 2010; Suyker and Verma, 2012). Evapotranspiration generally varies from 400-800 kg H_2O m^{-2}, reflecting differences in atmospheric demand, soil moisture availability, and irrigation regimes (Stoy et al., 2019; Suyker and Verma, 2009). Consequently, WUE for maize falls within 2.5-5.0 gC kg^{-1} H_2O, with irrigated and moderately water-limited systems often showing enhanced WUE due to optimized stomatal regulation. However, under water stress conditions, reductions in carbon assimilation typically outweigh declines in ET, leading to decrease in WUE. Extensive EC observations allow thorough assessments of maize GPP, ET, and WUE under a wide range of pedo-climatic conditions. These evaluations are essential not only for enhancing crop physiological understanding, but also promotes sustainable water and carbon management in maize agro-ecosystems.

For instance, models that accurately represent carbon and/or water fluxes are essential for understanding ecosystem responses to changing environmental conditions. Such models not only reproduce surface flux dynamics but also enable diagnostic analyses to assess ecosystem sensitivity to water stress, irrigation management, and climate variability. Approaches for estimating carbon and/or water exchanges can be broadly categorized into four groups: (i) remote sensing-based methods that infer productivity and evapotranspiration from satellite observations (Goetz et al., 2009; Potter et al., 2003), (ii) data-driven or empirical approaches relying on statistical relationships between fluxes and environmental drivers (Papale and Valentini, 2003), (iii) traditional crop growth models, which primarily focus on biomass accumulation under prescribed management conditions based on simplified numerical approaches (Moharana et al., 2025), and (iv) process-based Surface Vegetation Atmospheric Transfer (SVAT) models that represent physiological and biogeochemical mechanisms (Knorr

https://doi.org/10.5194/egusphere-2026-3119
Preprint. Discussion started: 16 June 2026

and Heimann, 1995) including land surface models (LSMs) that explicitly couple biophysical, hydrological, and physiological processes within a physically consistent SVAT framework (Calvet, 2000; Noilhan and Planton, 1989). Among these, LSMs originally developed to represent land-atmosphere exchanges for numerical weather/climate prediction explicitly resolve energy balance, soil moisture variability, canopy resistance, and photosynthesis-transpiration interactions (Koster and Suarez, 1996; Liang et al., 1994). By incorporating local meteorological and vegetation characteristics, LSMs dynamically provide a relevant platform for investigating ecosystem-scale GPP, ET, and further WUE dynamics under contrasting hydroclimatic regimes.

Temperate regions play a dominant role in global carbon-water exchanges; however, cropping systems in these regions differ substantially from those in tropical semi-arid climates (Beer et al., 2010; Jung et al., 2010; Nelson et al., 2020). In temperate regions, maize is typically cultivated during the summer season, resulting in a single growing cycle per year under relatively stable climatic conditions. In contrast, tropical semi-arid regions, particularly under monsoonal-dependent conditions, often support two maize growing seasons annually: a rainfed monsoon crop and an irrigated winter crop. These systems are characterized by high atmospheric demand, strong intra-seasonal rainfall variability, and frequent soil moisture limitations (Trenberth, 2011; Wang-Erlandsson et al., 2014). Additionally, irrigation practices introduce complex and non-linear interactions between soil moisture availability and atmospheric demand, which are not adequately represented in models primarily developed for temperate systems. Despite the extensive cultivation of maize in semi-arid regions, the temporal dynamics of carbon-water exchanges in these agro-ecosystems remain insufficiently understood due to limited long-term in-situ observations (Scott et al., 2023). Therefore, applying and evaluating LSMs across contrasting temperate and tropical semi-arid climates is essential to (i) test the robustness of model parameterizations governing carbon-water coupling,

https://doi.org/10.5194/egusphere-2026-3119
Preprint. Discussion started: 16 June 2026

(ii) identify climate-specific sensitivities and structural limitations, and (iii) improve the transferability of calibrated parameters for regional-scale simulations. Such cross-climatic assessments are particularly critical for enhancing confidence in LSM-based predictions of GPP, ET, and WUE under future climate variability and irrigation adaptation scenarios.

The Interactions between Soil, Biosphere, and Atmosphere (ISBA) scheme is a one such SVAT model originally developed by (Noilhan and Planton, 1989) and implemented within the SURFEX land surface modelling platform developed and maintained by Meteo-France, the French Weather Forecast Institute (Masson et al., 2013). ISBA provides the land surface boundary conditions (energy, water, and carbon fluxes) required by atmospheric models for numerical weather prediction and climate simulations (Noilhan and Planton, 1989). In its classical formulation, ISBA solves a single composite soil-vegetation surface temperature, which limits the representation of heterogeneous canopy-soil thermal exchanges (Noilhan and Planton, 1989). To overcome this limitation, (Boone et al., 2017) introduced a Multi-Energy Balance (MEB) version, hereafter referred to as ISBA-MEB. The MEB configuration explicitly separates soil and vegetation energy budgets, allowing up to three distinct source temperatures and flux pathways. The ISBA-MEB framework has been extensively evaluated over grasslands and croplands, within the temperate climate of France (Boone et al., 2017; Dare-Idowu et al., 2021), irrigated and rainfed grasslands in Spain (Martí et al., 2026) and Olive orchards and wheat in Morocco (Aouade et al., 2020). However, its performance remains largely unexplored outside temperate climates, especially under tropical semi-arid conditions, where high vapor pressure deficit, strong radiation loads, episodic monsoon rainfall, and irrigation-induced soil moisture heterogeneity exert strong controls on carbon-water coupling.

In France, maize accounts for nearly 17% of total cereal production with cultivation over 1.52 million hectares, while consuming approximately 70-80% of irrigation water (Battude et al., 2017). Maize is predominantly cultivated during the summer season (May-August),

https://doi.org/10.5194/egusphere-2026-3119
Preprint. Discussion started: 16 June 2026

coinciding with peak atmospheric evaporative demand and reduced river flows, thereby exerting significant pressure on regional water resources. In contrast, India contributes nearly 10% of global maize production, with cultivation extending over 9 million hectares. Despite its extensive cultivation in both countries, the WUE of maize in both France (3.5 gC Kg^{-1} H_2O) and India (1.83 gC Kg^{-1} H_2O) remains below the global average (4-5 gC Kg^{-1} H_2O) (FAO, 2017; Sharma et al., 2018). In France, maize is predominantly cultivated under sprinkler irrigation systems, where water is applied from above the canopy as pressurized droplets. In contrast, maize cultivation in India has traditionally relied on continuous furrow irrigation (CFI), where water is conveyed through furrows and allowed to infiltrate laterally and vertically, leading to near-saturated conditions across the entire field. Under CFI, prolonged surface wetting and deep percolation often result in low WUE, with substantial non-productive losses through soil evaporation and drainage below the root zone. Recent precision and conservation-oriented irrigation strategies such as regulated deficit irrigation, conservation tillage, and alternate furrow irrigation (AFI) have emerged as promising approaches to enhance WUE while sustaining yields (Al-Kayssi, 2023; Li et al., 2007; Yang et al., 2012). Among these, AFI has demonstrated considerable potential in reducing total irrigation inputs without significant yield penalties (Kang et al., 1998, 2001). The AFI technique alternates wetting and drying of adjacent furrows, inducing controlled and moderate water stress that enhances stomatal regulation and improves WUE. As AFI fundamentally modifies soil moisture distribution, root water uptake patterns, and canopy physiological responses relative to CFI, its influence on coupled carbon-water exchanges remains insufficiently quantified. Therefore, a robust process-based modelling framework capable of explicitly resolving soil-plant-atmosphere interactions is essential to evaluate the eco-physiological implications of contrasting irrigation regimes across diverse hydroclimatic conditions. These irrigation-induced changes ultimately propagate through stomatal regulation, which governs both carbon

https://doi.org/10.5194/egusphere-2026-3119
Preprint. Discussion started: 16 June 2026

assimilation and transpiration at the leaf and ecosystem scales. However, stomatal regulation is a complex biological process that cannot be fully constrained by fundamental physical conservation laws alone (Buckley, 2017; Cowan and GD, 1977; Medlyn et al., 2011), and it dynamically responds to radiation, vapour pressure deficit (VPD), and soil moisture conditions. Consequently, process-based diagnostics are required to rigorously evaluate model performance in capturing carbon-water coupling. As transpiration increases with atmospheric dryness, direct GPP-ET relationships may primarily reflect atmospheric demand rather than intrinsic physiological regulation. To address this, the underlying water use efficiency (uWUE) framework (Zhou et al., 2014) was adopted, wherein GPP was normalized by $VPD^{0.5}$ to account for the theoretically predicted inverse square-root dependence of stomatal conductance on VPD derived from optimal stomatal theory. This normalization reduces the first-order atmospheric demand effect on transpiration, thereby enabling a more physiologically meaningful assessment of intrinsic carbon-water coupling.

A systematic survey of the Scopus database (2004-2024) using keywords: "*ecosystem modelling*", *"modelling GPP and ET"*, *"modelling WUE"*, and *"land surface modelling on WUE"* revealed a clear research gap. Only a limited number of studies have addressed the modelling of GPP (4) and ET (10), while no study has examined ecosystem-scale WUE using a locally calibrated land surface model under contrasting climatic regimes. Notably, no study has simultaneously quantified WUE under contrasting irrigation treatments, particularly in Indian semi-arid agro-ecosystems where irrigation strongly regulates carbon-water coupling. Specifically, this study is aimed to: (i) characterize the dynamics of GPP, ET, and WUE of maize across both climates (temperate: France; tropical semi-arid: India), (ii) simulate these fluxes using the ISBA-A-g_s SVAT model with site-specific calibration and validation, (iii) analyse model sensitivity to climate-specific parameterization and its influence on model simulations, and (iv) perform diagnostic analyses to assess the model's ability to reproduce

https://doi.org/10.5194/egusphere-2026-3119
Preprint. Discussion started: 16 June 2026

underlying eco-physiological mechanisms governing WUE. To achieve these, comprehensive field measurements of GPP, ET, and WUE were considered in maize cultivated under contrasting climatic conditions subjected to different irrigation treatments.

This paper is organised as follows: (i) description of experimental sites and data collection, (ii) land surface model implementation, (iii) model simulations and validation, and (iv) diagnostic analysis on model simulations.

2.0 Material and Methods

2.1 Experimental sites description

2.1.1 Lamasquere, France (FR-Lam)

The Lamasquere experimental site (FR-Lam; 43°50′05″ N, 1°24′19″ E; 180 m above mean sea level) covers a flat area of approximately 24 ha, surrounded on its west and south sides by forest and is located about 25 km southwest of Toulouse, France (Figure 1). FR-Lam is a Class 1 ecosystem station within the Integrated Carbon Observation System (ICOS) network and is also part of the regional Spatial Observatory (OSR) project. The experimental field is situated along the Touch River and is characterized by a soil texture consisting of 54.3% clay, 33.7% loam, and 12% sand, rather homogeneous vertically up to 1m deep. According to the Köppen-Geiger climate classification, FR-Lam is categorized as a temperate oceanic climate (Cfb) (Kottek et al., 2006). Despite a mean annual precipitation of 642 mm and a mean annual air temperature of 16.2°C, precipitation is not evenly distributed throughout the year. In particular, summer periods can experience pronounced drought and heatwave conditions, leading to elevated VPD (~0.60 to 0.72 kPa) and reduced soil moisture availability. The regional wind regime is dominated by westerly and south-easterly winds, with an average wind speed of about 1.8 m s^{-1}. The site follows a regular 2-year crop rotation with wheat in the first year and intermediate cover followed by maize (summer crop) in the second year. Therefore,

https://doi.org/10.5194/egusphere-2026-3119
Preprint. Discussion started: 16 June 2026

only years cultivated with maize were selected for this study (2006, 2008, 2010, 2012, 2014, and 2015). Summer maize (silage) is generally sown between April and May, irrigated during the mid-season, and harvested from late August to early September. A shift in cultivar occurred during the 2014 and 2015 maize growing seasons. Pivot irrigation was applied during 2008 and 2010, whereas sprinkler irrigation was adopted in the remaining years. Details of the crop cycles and associated biophysical variables for the selected seasons are provided in Table 1.

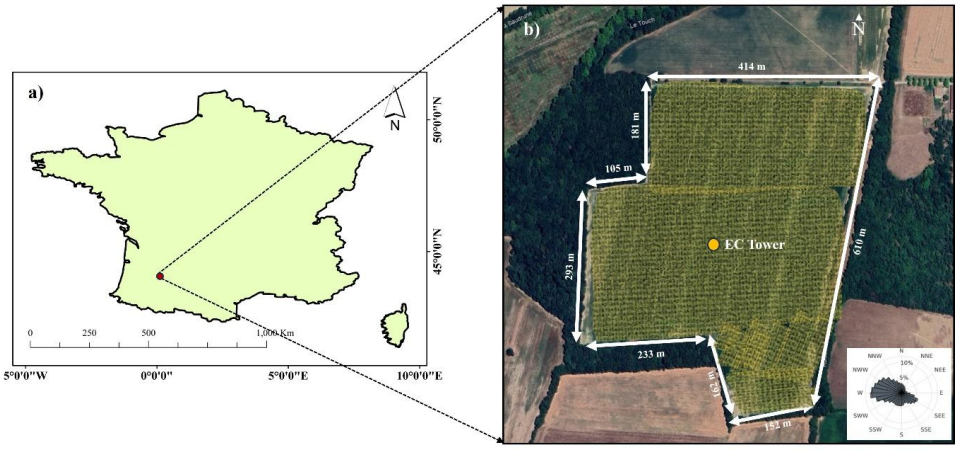

Figure 1. Overview of the FR-Lam experimental site: **(a)** Location of the study site; **(b)** Field extent and position of the EC tower within the site (Inset: observed wind rose diagram). Map source: The base map was designed and developed by Esri | Powered by Esri.

Table 1. Maize crop cycles with total rainfall and irrigation, sowing and harvest dates, crop length and maximum leaf area index (LAI) at FR-Lam experimental site.

Crop season	Rain [mm]	Irrigation [mm]	Total water [mm]	Sowing Date [DD/MM/YYYY]	Harvest Date [DD/MM/YYYY]	Crop length [Days]	Max LAI [m^2 m^{-2}]	Atmospheric evaporative demand ET_0 [mm]
2006	265.5	45.25	310.75	01/05/2006	31/08/2006	123	3.1	403

https://doi.org/10.5194/egusphere-2026-3119
Preprint. Discussion started: 16 June 2026

2008	269.67	27.30	296.97	20/05/2008	11/09/2008	124	3.8	363
2010	196.61	106.10	302.61	21/04/2010	20/09/2010	138	4.0	432
2012	410.07	148.70	558.07	27/04/2012	23/08/2012	122	5.8	374
2014	331.05	167.70	498.05	14/05/2014	22/09/2014	131	5.2	388
2015	354.41	120.00	474.41	05/05/2015	08/09/2015	128	6.6	435

2.1.2 Hyderabad, India (Ind-IITH)

Field experiments were conducted at the Ind-IITH site (17°35′48.44″ N, 78°07′05.78″ E; 549 m above mean sea level) in two adjacent agricultural fields located approximately 2 km from the Indian Institute of Technology Hyderabad (IITH), Telangana, India (Figure 2). Each field measures 100 m in length × 62 m in width, covering an area of about 0.62 ha. According to the Köppen-Geiger climate classification, the region falls under a tropical savannah climate (Aw), characterized by long dry periods and a short, intense wet season (Kottek et al., 2006). The soil at the experimental site consists of 10% clay, 15% loam, and 60% sand, exhibiting vertical homogeneity up to 1m deep. Mean annual precipitation ranges from 880 to 920 mm, with approximately 70% of the rainfall occurring during the southwest monsoon period (June-September). The average daily air temperature varies between 32 to 40°C during summer (April-June) and 22 to 24°C during winter (December-February), while VPD ranges from 1.11 kPa in summer to 2.72 kPa in winter. The regional wind regime is dominated by strong easterly winds, with a mean wind speed of approximately 1.05 m s^{-1}. Cropping patterns in the region are largely confined to two seasons, namely: the monsoon (kharif) and winter (rabi). During the monsoon season, maize is typically sown in mid-June and harvested by early October, whereas winter maize is sown in early December and harvested by early April. Two EC towers considering irrigation treatments: one for alternate furrow irrigation (AFI) and another for

https://doi.org/10.5194/egusphere-2026-3119
Preprint. Discussion started: 16 June 2026

continuous furrow irrigation (CFI) were installed each field. Under CFI, irrigation water is applied uniformly to all furrows, while under AFI, irrigation alternates between furrows based on the prevailing soil moisture conditions. Details of the crop cycles and associated biophysical variables for the selected seasons are summarized in Table 2.

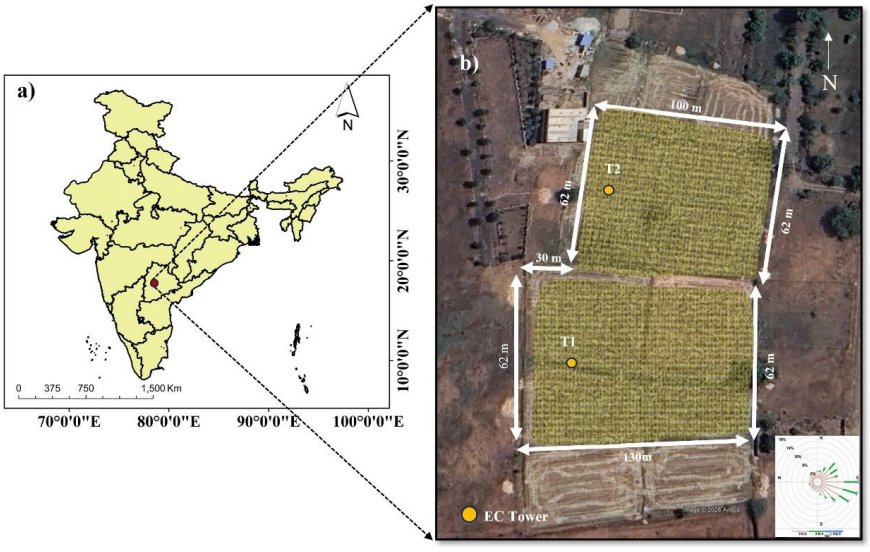

Figure 2. Overview of the Ind-IITH experimental site: **(a)** Location of the study site; **(b)** Field extent and position of the EC towers within the site (Inset: Observed Windrose diagram). Map source: The base map was designed and developed by Esri | Powered by Esri.

Table 2. Maize crop seasons with irrigation method, total rainfall and irrigation, sowing and harvest dates, crop length and maximum leaf area index (LAI) at Ind-IITH experimental site.

Crop season	Irrigation method	Rain [mm]	Irrigation [mm]	Sowing Date [DD/MM/YYYY]	Harvest Date [DD/MM/YYYY]	Crop length [Days]	Max LAI [m^2 m^{-2}]	Atmospheric evaporative demand ET_o [mm]

https://doi.org/10.5194/egusphere-2026-3119
Preprint. Discussion started: 16 June 2026

Monsoon	CFI	509	47	22/06/2024	05/10/2024	110	2.4	620
Monsoon	AFI	509	42	22/06/2024	05/10/2024	110	2.3	620
Winter	CFI	0	353.4	25/11/2024	10/04/2025	136	3.5	705
Winter	AFI	0	353.4	25/11/2024	10/04/2025	136	3.4	705

2.2 Field measurements

2.2.1 Eddy Covariance and Meteorological Datasets

At the FR-Lam site, an eddy covariance (EC) system was installed at 3.65m above ground level. The system comprised a three-dimensional sonic anemometer (CSAT-3; Campbell Scientific Inc., USA) and an open-path infrared gas analyser (LI-7500; LI-COR Inc., USA). Turbulent fluxes of CO_2 and H_2O were measured at 20 Hz using a datalogger (CR3000; Campbell Scientific Inc., USA) and subsequently averaged over a 30-minute interval. High-frequency raw data were processed using the EdiRe software following the CarboEurope-IP protocol (Aubinet et al., 1999) and the FLUXNET2015 processing guidelines (Pastorello et al., 2020). After standard quality control procedures, net ecosystem exchange (NEE) was calculated as the sum of turbulent CO_2 flux and the CO_2 storage term within the canopy. NEE was further partitioned into ecosystem respiration (R_{eco}) and gross primary productivity (GPP) using the method proposed by (Reichstein et al., 2005). This partitioning method had been optimized for croplands by (Béziat et al., 2010) (see also (Pique et al., 2020) for further details).

https://doi.org/10.5194/egusphere-2026-3119
Preprint. Discussion started: 16 June 2026

Flux footprint estimates were derived using the analytical model of (Kljun et al., 2004). Meteorological variables, including net radiation (CNR1; Kipp & Zonen), wind speed and wind direction (wind vane/propeller; R.M. Young), air temperature and relative humidity (HMP35; Vaisala), precipitation (ARG100 rain gauge), and diffuse and total photosynthetic active radiation (PAR) (BF3; Delta-T Devices Ltd., Cambridge, UK), were measured at a half-hourly interval. Ground heat flux was measured at a depth of 5cm using heat flux plates (HFP01; Hukseflux Thermal Sensors B.V., the Netherlands) and calculated as the average of four sensors installed around the EC tower. The soil heat storage was computed using the soil texture and soil water content to provide the total soil heat flux at the surface. The quality of the convective fluxes measured by the EC system was evaluated by estimating energy balance closure (see (Dare-Idowu et al., 2021)). Data points exhibiting poor closure (< 0.3) were excluded from the dataset to ensure the reliability of the flux measurements (Barr et al., 2006; Kidston et al., 2010). On average, 48% of the nighttime data was rejected due to insufficient turbulence. Soil temperature and volumetric soil water content were monitored at depths of 0, 5, 10, 30, 50, and 100 cm below soil surface. Measurements were performed using time-domain reflectometry probes (CS616; Campbell Scientific Inc., USA) from 2005 to 2011 and using Thetaprobe sensors (ML2X; Delta-T Devices Ltd., UK) from 2012 to 2015, with four replicated profiles distributed around the mast. A detailed description of the experimental setup and instrumentation is provided in (Béziat et al., 2010; Dare-Idowu et al., 2021).

At the Ind-IITH site, both experimental fields were equipped with open-path eddy covariance (EC) flux towers installed at a height of 2.2m above ground level. The EC system consisted of an open-path infrared gas analyser (IRGASON-EB-NC; Campbell Scientific Inc., USA) coupled with a 3D sonic anemometer (EC100; Campbell Scientific Inc., USA) for continuous measurements of CO_2 and H_2O fluxes. High-frequency raw data were recorded at 10 Hz using dataloggers (CR3000 and CR1000X; Campbell Scientific Inc., USA) and

https://doi.org/10.5194/egusphere-2026-3119
Preprint. Discussion started: 16 June 2026

subsequently averaged to a 30-minute interval. Raw EC data were processed using EasyFlux-PC software (Campbell Scientific Inc., USA). Detailed descriptions of data processing steps, quality control procedures, and flux corrections are provided in (Karimindla et al., 2024). Gap filling of missing flux data was performed using the 'REddyProc' package in the open-source 'R' environment, following the method proposed by (Reichstein et al., 2005). Net ecosystem exchange (NEE) was calculated as the sum of turbulent CO_2 fluxes and the CO_2 storage term within the canopy. NEE was further partitioned into ecosystem respiration (R_{eco}) and gross primary productivity (GPP) using the nighttime-based partitioning approach of (Reichstein et al., 2005). Flux footprint estimates were derived using the analytical model developed by (Kljun et al., 2004). Meteorological variables, including net radiation (CNR4; Campbell Scientific Inc., USA), air temperature and relative humidity (CS215 probe), wind speed and wind direction (propeller wind monitor; R.M. Young), and precipitation (TE525-L rain gauge; Campbell Scientific Inc., USA), were measured at 30-minute intervals. Soil heat flux (G) was measured using soil heat flux plates (HFP01SCL-PTL; Campbell Scientific Inc., USA) installed at a depth of 5 cm below the soil surface. Similar to FR-Lam, datapoints exhibiting poor closure (< 0.3) were excluded from the dataset to ensure the reliability of the flux measurements (Barr et al., 2006; Karimindla et al., 2024; Kidston et al., 2010). Soil volumetric water content and soil temperature at depths of 5, 10, and 30 cm were monitored using frequency-domain reflectometry sensors (TEROS-10; METER Group, USA) installed adjacent to the EC tower.

2.2.2 Vegetation characteristics and Irrigation inputs

At the FR-Lam site, vegetation leaf area index (LAI) was monitored during the peak growth period using a leaf area meter (LI-3100; LI-COR, Lincoln, NE, USA), following the methodology described by (Claverie et al., 2012). In addition, vegetation height (h_{veg}) and

https://doi.org/10.5194/egusphere-2026-3119
Preprint. Discussion started: 16 June 2026

aboveground biomass were measured on site from field sub-sampling and compared to the yield provided by the farmer. Information on irrigation timing and applied water amounts was collected through regular farmer surveys. A comprehensive description of vegetation monitoring protocols and management practices is provided in (Dare-Idowu et al., 2021) and (Pique et al., 2020). At the Ind-IITH site, LAI was measured from the tasselling to harvest stages using a plant canopy analyser (LI-2200C; LI-COR, Lincoln, NE, USA). Vegetation height was measured manually using a graduated ruler. Aboveground biomass and grain yield were determined at harvest from field sampling. Irrigation timing and applied water amounts were recorded on a daily basis for both CFI and AFI treatments.

2.3 Land surface model description and implementation

2.3.1 ISBA-A-g_s model description

The standard version of ISBA represents land surface heterogeneity using nineteen generic land cover types or patches: bare soil, rocks, ice and permanent snow, needleleaf trees, evergreen broadleaf trees, deciduous broadleaf trees, C3 crops, C4 crops, irrigated crops, herbaceous vegetation, tropical herbaceous vegetation, and wetlands (Calvet et al., 1998; Noilhan and Planton, 1989). In this study, ISBA was applied at a field scale (for which the cover is assumed to be homogeneous), and a single grid cell is characterized by a single dominant surface type (Noilhan and Planton, 1989). ISBA is implemented within the open-source SURFace EXternalisée (SURFEX) platform (version 9.1), developed by the Centre National de Recherches Météorologiques (CNRM) at Météo-France (Masson et al., 2013). In its standard configuration, leaf stomatal conductance is parameterized using the empirical approach of (Jarvis, 1976), which relies on multiplicative stress functions. While computationally efficient, this formulation has limitations in explicitly representing the physiological coupling between photosynthesis and stomatal regulation and doesn't account

https://doi.org/10.5194/egusphere-2026-3119
Preprint. Discussion started: 16 June 2026

for the direct effects of atmospheric CO_2 concentration on carbon assimilation and stomatal conductance. To overcome these limitations, ISBA was revised by (Calvet et al., 1998) through the incorporation of an optional photosynthesis-based stomatal conductance scheme, commonly referred to as the 'A-g_s' model, originally proposed by (Jacobs et al., 1996). This revised formulation explicitly links stomatal conductance to leaf-level photosynthetic activity, allowing a more mechanistic representation of CO_2 assimilation and stomatal regulation, and thereby improving the representation of vegetation-atmosphere carbon and water exchanges. In the Jacobs formulation, leaf-level carbon assimilation and stomatal conductance are simulated through a sequence of steps (described in Appendix A of (Calvet et al., 1998; Rivalland et al., 2005)), with the net assimilation rate (A_m) and stomatal conductance (g_s) expressed as:

$$A_m = A_{m,max}\left[1 - \exp\left(-\frac{g_m^*(C_i-\Gamma)}{A_{m,max}}\right)\right] \quad (1)$$

$$g_s = 1.6\, g_{sc} + g_c \quad (2)$$

where $A_{m,max}$ (mg m^{-2} s^{-1}) is the maximum photosynthetic rate, Γ(µmol mol^{-1}) is the CO_2 compensation concentration, g_m^* (m s^{-1}) is the unstressed mesophyll conductance, C_i(µmol mol^{-1}) is the intercellular CO_2 concentration, g_s (m s^{-1}) is the stomatal conductance, g_{sc} (m s^{-1}) is the stomatal conductance to carbon and g_c (m s^{-1}) is the cuticular conductance. Typical values of $A_{m,max}$ for C3 and C4 crops, data are provided in (Calvet, 2000).

Radiative transfer scheme is applied to upscale these carbon and water fluxes to the canopy scale, following the approaches of (Jacobs, 1994) and (Roujean, 1996). At the canopy level, gross primary productivity (GPP; g C m^{-2} s^{-1}) and evapotranspiration (ET; kg H_2O m^{-2} s^{-1}) are simulated, and water use efficiency (WUE) is then computed as a ratio of GPP to ET on a daily scale:

$$\text{WUE (g C kg } H_2O^{-1}) = \frac{\text{GPP}}{\text{ET}} \quad (3)$$

https://doi.org/10.5194/egusphere-2026-3119
Preprint. Discussion started: 16 June 2026

406

407 2.3.2 Model implementation

408 In this study, the non-interactive vegetation option of ISBA-A-g_s is employed, the key
409 vegetation characteristics: leaf area index (LAI), vegetation height (h_{veg}), and fractional
410 vegetation cover (F_C) are prescribed using *in situ* measurements rather than simulated
411 dynamically. The multilayer soil diffusion (DIF) scheme is adopted to simulate vertical
412 transfers of soil moisture and heat within the soil profile (Decharme et al., 2026). Within the
413 SURFEX framework, land surface parameters and ancillary variables are typically derived
414 from the ECOCLIMAP II database (Faroux et al., 2013). However, as the present study focuses
415 on ecosystem-scale simulations and benefits from detailed field observations, the default
416 ECOCLIMAP II parameterization is bypassed, and site-specific in situ measurements are used
417 to constrain the model configuration.

418 The main input parameters and state variables used in the model simulations for the FR-
419 Lam and Ind-IITH sites are summarized in Tables 3 and 4, respectively. At both sites,
420 vegetation characteristics including leaf area index (LAI), canopy height (h_{veg}), and fractional
421 vegetation cover (F_c) were prescribed from in-situ measurements at 10-day intervals. Surface
422 roughness length was estimated as a fixed fraction of canopy height ($0.15 \times h_{veg}$). In this study,
423 patch 8, representing C4 crops, was employed to simulate the maize crop at both sites. The
424 model was forced with half-hourly meteorological observations, including air temperature (TA,
425 K), specific humidity (QA, kg kg^{-1}), surface air pressure (PS, Pa), incoming longwave radiation
426 (LWin, W m^{-2}), wind speed (WS, m s^{-1}), wind direction (degrees), ambient CO_2 concentration
427 (kg m^{-3}), rainfall (RAIN, kg m^{-2}), and incoming shortwave radiation (SWin, W m^{-2}). The
428 multilayer soil diffusion scheme requires information on soil stratification; accordingly, eight
429 soil layers were defined at depths of 0, 5, 10, 30, 50, 100, and 150 cm below the ground surface.
430 Soil hydraulic conductivity was estimated using pedotransfer functions based on measured

https://doi.org/10.5194/egusphere-2026-3119
Preprint. Discussion started: 16 June 2026

sand and clay contents at the respective depths (Cosby et al., 1984). Initial soil moisture and soil temperature profiles were prescribed using in-situ observations. Surface albedo during active sunshine hours (10:00-15:00 local time) is provided to minimize the influence of low solar zenith angles, following (Kalma and Stanhill, 1969). Subsequently, total surface albedo was partitioned into soil (alb_{soil}) and vegetation (alb_{veg}) components using a fractional weighting approach based on F_C. Model simulations were constrained to the crop growth period by prescribing site-specific sowing and harvesting dates in the forcing files.

Table 3. Values and ranges of ISBA-A-g_s model input variables considered at FR-Lam experimental site.

Description	Symbol	Range	Unit	Reference
Leaf area index	LAI	0-6.8	[m^2 m^{-2}]	Measured
Minimum Leaf Area Index	LAI_{Min}	0.1-0.4	[m^2 m^{-2}]	Measured
Vegetation Height	h_{veg}	0-3.3	[m]	Measured
Fractional vegetation cover	F_c	0-1.0	-	Estimated
Vegetation albedo	alb_{veg}	0.16-0.21	-	Derived from measurement
Soil albedo	alb_{soil}	0.12-0.16	-	Derived from measurement
Max solar radiation available for photosynthesis	R_{GL}	80-100	[W m^{-2}]	(Moigne and Boone, 2012)
Vegetation emissivity	$Emis_{veg}$	0.97	-	-
Soil albedo	$Emis_{soil}$	0.90	-	-
Clay fraction	CI	0.54	-	Measured

https://doi.org/10.5194/egusphere-2026-3119
Preprint. Discussion started: 16 June 2026

Sand fraction	Sd	0.12	-	Measured
Mesophyll conductance	gm	0.001-0.03	[m s^{-1}]	(Calvet, 2000)
Minimum stomatal resistance	RSMIN	40	[s m^{-1}]	(Calvet, 2000)
Cuticular conductance	GC	0.00015 – 0.00030	[m s^{-1}]	(Gibelin et al., 2006)
Critical normalized soil water content for stress parameterization	F2I	0.2 – 0.5	-	(Calvet, 2000)
Ecosystem respiration parameter	RE25	0.0000002 – 0.0000003	[kg/kgms^{-1}]	(Gibelin et al., 2006)
Maximum leaf to air saturation deficit	D_{Max}	0.05 – 0.5	[kg kg^{-1}]	(Calvet, 2000)
Vegetation thermal inertia coefficient	C_V	0.00005	[K m^{-2} J^{-1}]	(Noilhan and Planton, 1989)
Coeff for max inter water storage capacity	WR_{Max}	0.05 – 0.3	-	(Moigne and Boone, 2012)
Ratio of surface roughness lengths	Z_o-Z_H	7 – 10	-	(Boone et al., 2017)

Table 4. Values and ranges of ISBA-A-g_s model input variables considered at Ind-IITH experimental site.

Description	Symbol	Range	Unit	Reference
Leaf area index	LAI	0-3.6	[m^2 m^{-2}]	Measured
Minimum Leaf Area Index	LAI_{Min}	0.1-0.4	[m^2 m^{-2}]	Measured
Vegetation Height	h_{veg}	0-2.71	[m]	Measured
Fractional vegetation cover	F_c	0-1.0	-	Estimated

https://doi.org/10.5194/egusphere-2026-3119
Preprint. Discussion started: 16 June 2026

Vegetation albedo	alb_{veg}	0.16-0.18	-	Derived from measurement
Soil albedo	alb_{soil}	0.12-0.15	-	Derived from measurement
Max solar radiation available for photosynthesis	R_{GL}	80-200	[W m^{-2}]	Derived from measurement
Vegetation emissivity	$Emis_{veg}$	0.96	-	-
Soil albedo	$Emis_{soil}$	0.90	-	-
Clay fraction	CI	0.10	-	Measured
Sand fraction	Sd	0.60	-	Measured
Mesophyll conductance	gm	0.001-0.03	[m s^{-1}]	(Calvet, 2000)
Minimum stomatal resistance	RSMIN	37	[s m^{-1}]	(Calvet, 2000)
Cuticular conductance	GC	0.00015 – 0.00030	[m s^{-1}]	(Gibelin et al., 2006)
Critical normalized soil water content for stress parameterization	F2I	0.21 – 0.48	-	(Calvet, 2000)
Ecosystem respiration parameter	RE25	0.0000002 – 0.0000003	[kg/kgms^{-1}]	(Gibelin et al., 2006)
Max leaf to air saturation deficit	D_{Max}	0.05 – 0.45	[kg kg^{-1}]	(Calvet, 2000)
Vegetation thermal inertia coefficient	C_V	0.00005	[K m^{-2} J^{-1}]	(Noilhan and Planton, 1989)
Coeff for max inter water storage capacity	WR_{Max}	0.05 – 0.35	-	(Moigne and Boone, 2012)

https://doi.org/10.5194/egusphere-2026-3119
Preprint. Discussion started: 16 June 2026

Ratio of surface roughness lengths	Z_o-Z_H	7 – 10	-	(Boone et al., 2017)

442

443 **2.4 Model calibration and validation**

444 To achieve an optimal balance between the large number of input parameters in ISBA-A-
445 g_s and the available computational resources, a stepwise calibration strategy was adopted.
446 Based on previous studies and expert knowledge of the model, 12 parameters (gm, GC, F2I,
447 RE25, D_{Max}, C_V, LAI_{Min}, R_{GL}, RSMIN, WR_{Max}, and Z_o-Z_H) potentially influencing GPP and
448 ET were initially selected (Aouade et al., 2020; Boone et al., 2017; Dare-Idowu et al., 2021) .
449 A 'one-at-a-time' sensitivity analysis was then performed to isolate the effect of each
450 parameter. Simulations were conducted for three maize growing seasons (2008, 2010, and
451 2012) at the FR-Lam site and for four treatments (2 seasons) at the Ind-IITH site. For each
452 parameter, a realistic range was defined based on literature values, and 50 simulations were
453 performed per parameter for each crop year. Model performance was evaluated by comparing
454 simulated GPP, ET, and WUE fluxes with in-situ observations using the root mean square error
455 (RMSE) and the coefficient of determination (R^2). The performance metrics were ranked by
456 minimizing RMSE and maximizing R^2, and a Pareto-based multi-objective approach (Demarty
457 et al., 2005) was used to partition simulations into acceptable and non-acceptable parameter
458 sets. To quantify parameter sensitivity, the cumulative distributions of acceptable and non-
459 acceptable parameter values were compared using the Kolmogorov-Smirnov (KS) test, which
460 provides a probability value describing the statistical separation between the two distributions.
461 The optimized parameter set was subsequently validated using independent crop years (FR-
462 Lam: 2006, 2014, and 2015; Ind-IITH: two seasons) not included in the calibration phase.

463

464 **2.5 Model assessment**

https://doi.org/10.5194/egusphere-2026-3119
Preprint. Discussion started: 16 June 2026

Model performance in reproducing GPP, ET, and WUE was evaluated using three goodness-of-fit indicators. EC flux-tower measurements were used as the reference for model validation. The selected indicators quantify the strength of association, residual errors, and systematic bias between observations and simulations. These metrics were computed using paired EC-observed values (O_i) and ISBA-A-g_s simulated values (P_i) of GPP, ET, and WUE, along with their respective means ($\bar{O}$ and $\bar{P}$), during crop growth seasons. Model performance was assessed using the coefficient of determination (R^2), the root mean square error (RMSE), and the percentage bias (PBIAS).

i. The coefficient of determination (R^2) quantifies the strength of the linear association between observed and simulated fluxes:

$$R^2 = \left\{ \frac{\sum_{i=1}^{n}(O_i-\bar{O})(P_i-\bar{P})}{[\sum_{i=1}^{n}(O_i-\bar{O})^2]^{0.5}\,[\sum_{i=1}^{n}(P_i-\bar{P})^2]^{0.5}} \right\}^2 \quad (4)$$

ii. RMSE provides a measure of the overall magnitude of simulation errors.

$$RMSE = \left[\frac{1}{n}\sum_{i=1}^{n}(P_i - O_i)^2\right]^{0.5} \quad (5)$$

iii. PBIAS indicates the average tendency of the model to overestimate or underestimate the observed values.

$$PBIAS = 100\,\frac{\sum_{i=1}^{n}(O_i - P_i)}{\sum_{i=1}^{n} O_i} \quad (6)$$

To further perform diagnostic analysis, the relationship between $GPP \cdot VPD^{0.5}$ and ET was examined using both observations and model simulations. This analysis was restricted to periods of peak leaf area index (LAI > 1.5 $m^2\ m^{-2}$) to minimize soil evaporation contributions and isolate canopy-level stomatal behaviour. Additionally, the response of evaporative fraction ($EF = \frac{LE}{H+LE}$) to VPD was analysed using half-hourly averages during peak photosynthetic periods (11:00-15:00) within the active growing phase.

https://doi.org/10.5194/egusphere-2026-3119
Preprint. Discussion started: 16 June 2026

3.0 Results

3.1 Sites meteorology and vegetation characteristics

Monthly variations in major meteorological variables, including rainfall (P), air temperature (TA), and vapor pressure deficit (VPD), along with leaf area index (LAI) observed at the FR-Lam site across six maize growing seasons, are presented in Figure 3. Rainfall exhibited pronounced seasonality, with peak precipitation occurring during April and May (mean ± standard deviation: 69.29 ± 43.86 mm), characterizing these months as relatively wet, followed by a marked decline during summer (July and August), representing comparatively drier conditions. Among the seasons, 2008 received the lowest rainfall (270 mm), whereas 2012 recorded the highest (410 mm), corresponding to distinctly dry and wet years, respectively. Supplemental irrigation was primarily required during July and August (393 mm), coinciding with the peak vegetative growth stage (dough) for all the years. The balance between total available water (precipitation + irrigation) and atmospheric evaporative demand (ET_o) further highlighted interannual contrasts, with positive (+184 mm) and negative (-66 mm) water surpluses observed during 2012 and 2008, respectively. The period (April to September) was characterized by a progressive transition from relatively wet conditions in spring to drier and warmer conditions during mid to late summer, leading to increased atmospheric demand. Seasonal mean air temperature ranged from 17 ± 1.60°C in 2012 to 19.50 ± 1.20°C in 2008, consistent with rainfall-driven wet and dry classifications. Similarly, mean VPD varied from 0.67 ± 0.10 kPa in 2012 to 0.78 ± 0.10 kPa in 2008, indicating greater atmospheric water demand in dry seasons. LAI displayed strong seasonal variability, with lower values observed in 2006 (3.1 m^2 m^{-2}), 2008 (3.9 m^2 m^{-2}), and 2010 (4 m^2 m^{-2}) compared to later years (2012: 5.9 m^2 m^{-2}; 2014: 5.2 m^2 m^{-2}; 2015: 6.6 m^2 m^{-2}). Despite relatively dry conditions in 2010, early sowing (21st April) along with the onset of rainfall facilitated canopy development and higher LAI, underscoring the combined influence of climatic conditions and management practices

https://doi.org/10.5194/egusphere-2026-3119
Preprint. Discussion started: 16 June 2026

on crop growth. In contrast, the lower LAI in 2008 was attributed to elevated temperatures and increased atmospheric water stress due to delayed sowing (20th May). Peak LAI generally coincided with irrigation-intensive months (July and August), reflecting adequate soil moisture availability during critical growth stages. Overall, the FR-Lam site exhibited pronounced seasonal and interannual variability, with relatively drier conditions during the early seasons (2006, 2008, and 2010) and wetter conditions in later years (2012, 2014, and 2015). In addition to climatic variability, a change in maize cultivar during 2014 and 2015 contributed to improved canopy development and higher yield, indicating that both environmental conditions and management practices influenced crop performance.

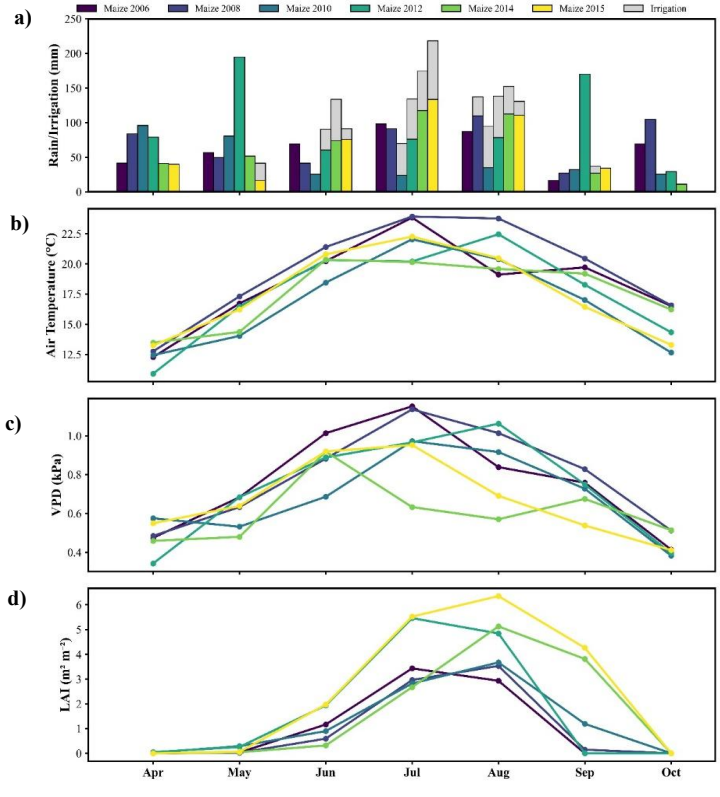

https://doi.org/10.5194/egusphere-2026-3119
Preprint. Discussion started: 16 June 2026

Figure 3. Monthly variations in environmental variables, including rainfall/Irrigation (cumulative values) **(a)**; Air temperature **(b)**; Vapor pressure deficit **(c)**; and Leaf are index **(d)** observed at FR-Lam experimental site during maize growing seasons.

At the Ind-IITH site, the data were collected between June 2024 and April 2025, so the focus is restricted to seasonal variations. The major meteorological variables including rainfall, air temperature, and vapor pressure deficit, along with leaf area index observed during the monsoon and winter seasons are presented in Figure 4. Rainfall was majorly concentrated during the monsoon season (June-August), with a total of 509 mm. During the monsoon, three irrigation events totalling 46.8 mm were applied, primarily during the dough (grain filling stage) and maturity stages. Despite this additional input, the balance between total available water (precipitation/irrigation) and atmospheric evaporative demand (ET_o) remained negative, with deficits of -64 mm and -81 mm under CFI and AFI treatments, respectively. In contrast, the winter season recorded zero rainfall, making the crop fully dependent on irrigation. Total irrigation supplied during winter amounted to 543 mm under CFI and 453 mm under AFI. Even with these inputs, substantial water deficits persisted, with total available water falling short of ET_o by -163 mm (CFI) and -252 mm (AFI). The marked contrast in rainfall distribution between monsoon and winter seasons highlights the distinctly different seasonal irrigation strategies followed at the Ind-IITH site. During the monsoon, temperature variability was relatively low (1.20°C), with an average of 28.23°C. In contrast, winter temperatures were initially moderate (25.63°C) but increased progressively, rising at approximately 2.88°C Day^{-1} to reach a peak of 38.63°C toward the end of the season. VPD variations closely followed temperature patterns, with mean values of 1.12 kPa and 2.73 kPa during the monsoon and winter seasons, respectively. Average LAI was lower during the monsoon (1.33 m^2 m^{-2}) compared to winter (1.97 m^2 m^{-2}), likely influenced by seasonal differences in radiation and atmospheric conditions. Overall, the monsoon period exhibited relatively stable temperatures

https://doi.org/10.5194/egusphere-2026-3119
Preprint. Discussion started: 16 June 2026

and lower VPD, whereas the winter season experienced progressively increasing temperatures and substantially higher VPD, indicating greater atmospheric water demand and the necessity of analysing WUE dynamics separately for monsoon and winter growing seasons.

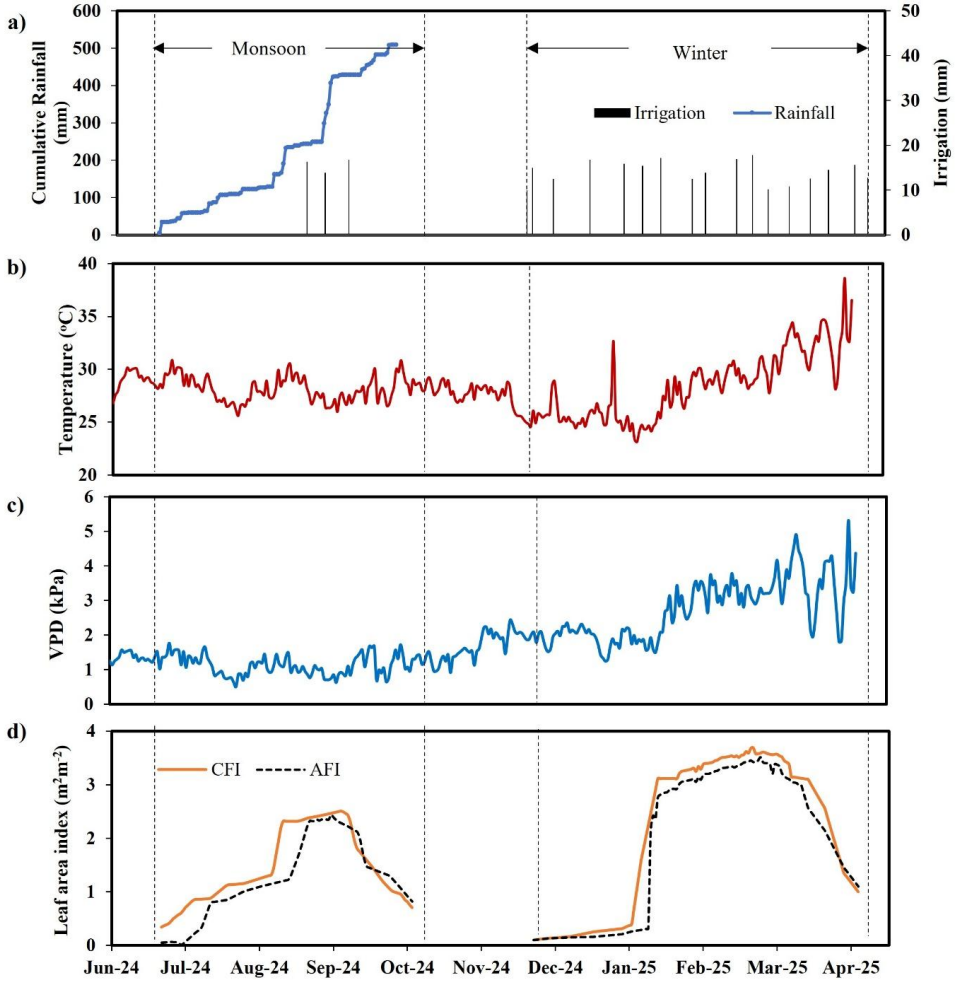

Figure 4. Seasonal variations in environmental variables, including cumulative rainfall and Irrigation **(a)**; Air temperature **(b)**; Vapor pressure deficit **(c)**; Leaf are index **(d)** observed at Ind-IITH experimental site during maize growing seasons.

A comparative analysis of meteorological conditions between the FR-Lam and Ind-IITH sites reveals that the climate variability at the FR-Lam site was primarily expressed

https://doi.org/10.5194/egusphere-2026-3119
Preprint. Discussion started: 16 June 2026

between years, distinguishing relatively dry (e.g., 2008) and wet (e.g., 2012) seasons, while maintaining a consistent growing period from April to September with moderate fluctuations in rainfall and VPD. In contrast, the Ind-IITH site exhibited pronounced intra-annual variability, with a sharp transition between monsoon and winter seasons. Rainfall was concentrated during the monsoon, whereas winter conditions were entirely irrigation-driven, resulting in contrasting water availability regimes. These seasonal differences were further amplified by atmospheric demand, with substantially higher VPD observed during winter compared to the relatively stable monsoon period. Importantly, the seasonal contrasts at Ind-IITH exceeded the interannual variability observed at FR-Lam, particularly in cumulative rainfall and VPD. While FR-Lam showed moderate year-to-year differences in precipitation, Ind-IITH exhibited a near-complete shift from water-abundant to water-deficient conditions between seasons, along with a marked increase in VPD. These differences were also reflected in canopy development, where LAI variability at FR-Lam was linked to both climatic conditions and management factors (e.g., sowing date and cultivar change), whereas at Ind-IITH, LAI differences were mainly driven by seasonal contrasts in radiation, temperature, and water availability. Overall, climatic variability at Ind-IITH is substantially greater at the seasonal scale, especially for VPD and water inputs, with important implications for crop water use and WUE dynamics.

3.2 Dynamics of gross primary productivity, evapotranspiration, and water use efficiency

Seasonal boxplots revealed substantial interannual variability in gross primary productivity (GPP), evapotranspiration (ET), and water use efficiency (WUE) estimated across the six maize growing seasons at the FR-Lam site and the two seasons at the Ind-IITH site with the 2 irrigation treatments (Figure 5). At FR-Lam, the seasonal mean GPP ranged from -8 to -11 gC m^{-2} day^{-1}, with the strongest carbon uptake observed in 2012 and 2015 (-10 to -11 gC m^{-}

https://doi.org/10.5194/egusphere-2026-3119
Preprint. Discussion started: 16 June 2026

^{2} day^{-1}). In contrast, 2010 exhibited comparatively lower GPP (-6 gC m^{-2} day^{-1}). These results demonstrate marked interannual differences in seasonal carbon assimilation. Seasonal ET varied between 3.5 to 5.8 kg H_2O m^{-2} day^{-1}. The maximum ET occurred in 2015, accompanied by the largest upper range values (12 kg H_2O m^{-2} day^{-1}) and the minimum ET observed in 2008 (3.5 kg H_2O m^{-2} day^{-1}). Across seasons, ET distributions showed substantial dispersion, reflecting strong variability in daily evaporative demand and canopy water flux. WUE ranged from 1.6 to 2.6 gC kg^{-1} H_2O over the seasons. Peak WUE was recorded in 2008 (2.4-2.6 gC kg^{-1} H_2O), while 2010 and 2015 exhibited comparatively lower values (1.5-1.8 gC kg^{-1} H_2O). Despite high carbon uptake in 2012, WUE remained moderate due to concurrent increases in ET. At Ind-IITH, GPP ranged from 6 to 8 gC m^{-2} day^{-1}, with overlapping interquartile ranges between CFI and AFI during the monsoon. In Winter, GPP were of similar magnitude (5-7 gC m^{-2} day^{-1}), and variability remained substantial between the treatments. The distribution patterns indicate that the irrigation strategy had a limited influence on seasonal carbon assimilation compared to the intrinsic seasonal variability. In contrast, ET showed clear and consistent differences between irrigation treatments. During monsoon, CFI exhibited higher ET (4.5-5.0 kg H_2O m^{-2} day^{-1}) compared to AFI (3.0-3.5 kg H_2O m^{-2} day^{-1}). A similar reduction under AFI was observed during winter, and ET under CFI (4.5-5.0 kg H_2O m^{-2} day^{-1}) exceeded that under AFI (2.5-3.0 kg H_2O m^{-2} day^{-1}). These patterns indicate that AFI consistently reduced seasonal water loss relative to CFI. Despite similar magnitudes of GPP between treatments, AFI resulted in higher WUE in both seasons. During Monsoon, WUE under AFI ranged from 2.0 to 2.2 gC kg^{-1} H_2O, compared to 1.4 to 1.6 gC kg^{-1} H_2O under CFI. A comparable enhancement was observed in winter, with AFI maintaining higher WUE relative to CFI. The improvement in WUE under AFI primarily corresponded to reductions in ET rather than substantial differences in GPP. Overall, irrigation treatment in the Ind-IITH site exerted a stronger influence on ET and WUE than on GPP.

https://doi.org/10.5194/egusphere-2026-3119
Preprint. Discussion started: 16 June 2026

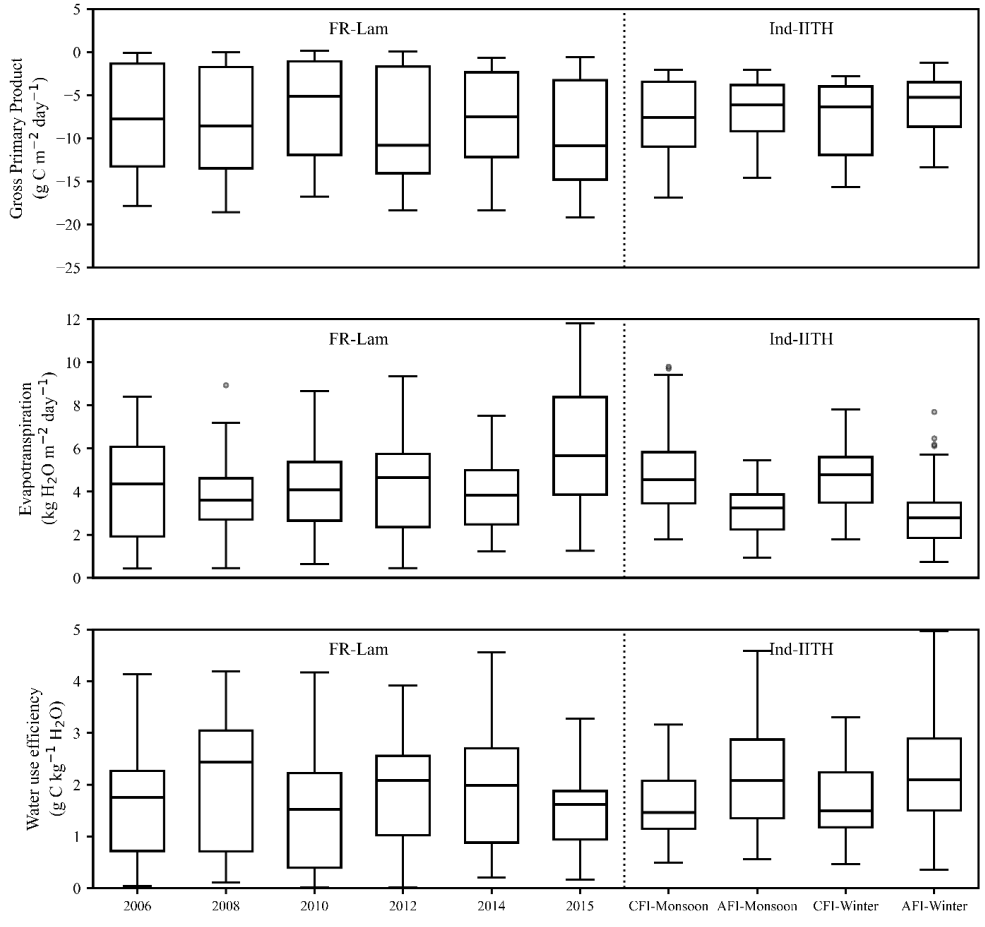

Figure 5. Seasonal variability of gross primary productivity (GPP), evapotranspiration (ET), and water use efficiency (WUE) during six maize growing seasons (2006, 2008, 2010, 2012, 2014, and 2015) at the FR-Lam site and four treatments considered at the Ind-IITH site.

A cross-site comparison further highlights that WUE variability emerges from different controlling mechanisms at FR-Lam and Ind-IITH, despite exhibiting comparable magnitudes overall. At FR-Lam, WUE was primarily governed by interannual climatic variability, with higher values observed during relatively warmer and drier years (e.g., 2008), where reduced ET relative to carbon uptake enhanced efficiency. In contrast, at Ind-IITH, WUE was more

https://doi.org/10.5194/egusphere-2026-3119
Preprint. Discussion started: 16 June 2026

strongly influenced by irrigation management than by seasonal carbon assimilation, with AFI consistently improving WUE compared to CFI through systematic reductions in ET while maintaining similar GPP levels. Despite these differing controls, the range of WUE values remained broadly similar between the temperate (FR-Lam) and semi-arid (Ind-IITH) environments, indicating that both climatic variability and irrigation strategies can lead to comparable ecosystem-scale efficiencies via different pathways. Notably, higher WUE under warmer conditions at FR-Lam and under water-saving irrigation (AFI) at Ind-IITH suggests that reductions in non-productive water losses play a key role in enhancing WUE across contrasting climates. Overall, these findings demonstrate that while WUE magnitude may be similar across sites, its underlying drivers differ fundamentally, being climate-driven at FR-Lam and management-driven at Ind-IITH.

3.3 Model calibration

Table 5 summarizes the calibrated parameter ranges, initial values, and optimal estimates of the ISBA-A-g_s model for the FR-Lam. Among the 12 parameters investigated, five parameters (gm, GC, F2I, RE25, and D_{Max}) were identified as particularly sensitive. Mesophyll conductance (gm) was explored within a range of 1×10^{-3} to 3×10^{-2} m s^{-1}, with an initial value of 7.53×10^{-2} m s^{-1} and converged to 2×10^{-3} m s^{-1}, which may indicate relatively moderate internal CO_2 diffusion constraints. The reduction from the initial value suggests tighter mesophyll limitation under site-specific environmental conditions. Cuticular conductance (GC) was varied between 1.5 to 4.5×10^{-4} m s^{-1}, with an optimal estimate of 4.2×10^{-4} m s^{-1}. The optimized value being close to the upper bound could imply a strong contribution of cuticular water loss to total transpiration, particularly under elevated atmospheric demand during dry seasons. The critical normalized soil water content for stress parameterization (F2I) converges to an optimal value of 0.334. This may suggest that soil moisture stress begins to

https://doi.org/10.5194/egusphere-2026-3119
Preprint. Discussion started: 16 June 2026

696 significantly regulate carbon-water flux coupling at one-third of normalized soil water
697 availability is depleted, reflecting moderate drought sensitivity. The ecosystem respiration
698 parameter at 25°C (RE25) was tested between 2 to 3 × 10^{-7} kg/kg m s^{-1}, with an optimal value
699 of 2.50 × 10^{-7} kg/kg m s^{-1} indicating stable temperature-normalized respiratory flux
700 representation. The maximum leaf to air saturation deficit (D_{Max}) was constrained between 0.05
701 and 0.5 kg kg^{-1}, with calibration yielding an optimal value of 0.065 kg $kg^{-1,}$ which may indicate
702 strong stomatal sensitivity to atmospheric VPD, consistent with observed transpiration
703 regulation under dry air conditions. Overall, the calibrated parameters reflect FR-Lam site is
704 characterized by moderate mesophyll diffusion capacity, appreciable cuticular conductance,
705 intermediate soil moisture stress sensitivity, stable respiratory scaling, and strong atmospheric
706 control on stomatal behaviour. These optimized values improved the representation of GPP,
707 ET, and WUE at the FR-Lam site, reducing bias and improving model-observation agreement
708 (Supplementary Table S1-S2).
709
710 **Table 5.** Calibrated ISBA-A-g_s model parameters for the FR-Lam experimental site.

Description	Symbol	Value Range	Initial value considered	Optimal Value	Reference
Mesophyll conductance	gm	1 × 10^{-3} - 3 × 10^{-2}	7.53 × 10^{-3}	2 × 10^{-3}	(Calvet, 2000)
Cuticular conductance	GC	1.5 - 4.5 × 10^{-4}	4 × 10^{-4}	4.2 × 10^{-4}	(Gibelin et al., 2006)
Critical normalized soil water content for stress parameterization	F2I	0.2 - 0.5	0.20	0.334	(Calvet, 2000)
Ecosystem respiration parameter	RE25	2 to 3 × 10^{-7}	2.88 × 10^{-7}	2.50 × 10^{-7}	(Gibelin et al., 2006)

https://doi.org/10.5194/egusphere-2026-3119
Preprint. Discussion started: 16 June 2026

Maximum leaf to air saturation deficit	D_{Max}	0.05 – 0.5	0.05	0.065	(Calvet, 2000)

Table 6 summarizes the calibrated parameter ranges, initial values, and optimal estimates of the ISBA-A-gs model for maize under CFI and AFI treatments during the monsoon and winter seasons at the Ind-IITH. Among the 12 parameters investigated, five (gm, GC, F2I, RE25, and D_{Max}) were identified as particularly sensitive. Mesophyll conductance (gm) exhibited lower optimized values under AFI compared to CFI during the monsoon (2.2×10^{-3} vs 2.5×10^{-3} m s^{-1}), indicating a mild limitation in internal CO_2 diffusion under partial root-zone drying. This reduction moderated GPP but limited excessive transpiration, thereby contributing to improved WUE under AFI (Al-Kayssi, 2023; Reavis et al., 2024). In contrast, marginally higher winter gm supported enhanced carbon gain under lower atmospheric demand. The GC remained within the lower range (2.9-3.5 $\times 10^{-4}$ m s^{-1}) across treatments, with marginally higher values under CFI during winter, reflecting slightly enhanced non-stomatal water loss under fully irrigated conditions. The F2I ranged between 0.400 and 0.412, with consistently higher values during winter, suggesting stronger soil moisture control on stomatal regulation in the dry season. The critical soil moisture threshold (F2I ≈ 0.40-0.41) exerted strong control on ET variability, particularly under AFI, indicating that the earlier stomatal regulation under declining soil moisture reduced transpiration without proportionally suppressing GPP. The 'RE25' varied from 2.20 to 2.40 $\times 10^{-7}$ kg/kg m s^{-1}, with slightly elevated values during winter, consistent with seasonal temperature regulation of respiration processes. The optimized D_{Max} values (0.070-0.075) indicated moderate atmospheric control, constraining ET under high VPD while stabilizing WUE. Overall, AFI treatments showed subtle reductions in gm and RE25, along with slight adjustments in soil moisture stress thresholds, reflecting physiological optimization under alternate wetting and drying conditions in the Indian semi-arid agroecosystem.

https://doi.org/10.5194/egusphere-2026-3119
Preprint. Discussion started: 16 June 2026

735

736 **Table 6.** Calibrated ISBA-A-g_s model parameters for the Ind-IITH experimental site.

Description	Symbol	Value Range	Initial value considered	Optimal Value				References
				CFI - Monsoon	AFI - Monsoon	CFI - Winter	AFI - Winter	
Mesophyll conductance	gm	1×10^{-3} - 3×10^{-2}	7.53×10^{-3}	2.5×10^{-3}	2.2×10^{-3}	2.8×10^{-3}	2.7×10^{-3}	(Calvet, 2000)
Cuticular conductance	GC	1.5 - 3.0 × 10^{-4}	4×10^{-4}	3×10^{-4}	2.9×10^{-4}	3.5×10^{-4}	3.2×10^{-4}	(Gibelin et al., 2006)
Critical normalized soil water content for stress parameterization	F2I	0.21 - 0.48	0.20	0.400	0.405	0.412	0.409	(Calvet, 2000)
Ecosystem respiration parameter	RE25	2 to 3 × 10^{-7}	2.88×10^{-7}	2.20×10^{-7}	2.22×10^{-7}	2.32×10^{-7}	2.40×10^{-7}	(Gibelin et al., 2006)
Maximum leaf to air	D_{Max}	0.05 - 0.45	0.04	0.070	0.071	0.075	0.071	(Calvet, 2000)

https://doi.org/10.5194/egusphere-2026-3119
Preprint. Discussion started: 16 June 2026

saturation

deficit

737

738 **3.4 Model performance over the FR-Lam site**

739 The calibrated ISBA-A-g_s model demonstrated strong potential in reproducing GPP,
740 ET, and WUE dynamics at the FR-Lam site (Figure 6). GPP was simulated with high accuracy
741 (R^2 ranging from 0.80 to 0.93) capturing both dry (2008) and wet (2014) conditions, indicating
742 robust representation of photosynthetic processes across moisture gradients. The low RMSE
743 and moderate PBIAS further confirm reliable simulation of seasonal carbon uptake, although
744 systematic overestimation was evident in 2014 (-28%) and 2015 (-16%), suggesting enhanced
745 modelled assimilation under non-water-limited conditions. ET simulations exhibited moderate
746 to strong agreement with observations (R^2 of 0.60 in 2012 to 0.86 in 2015), reflecting the
747 model's ability to reproduce canopy-atmosphere water exchange (Dare-Idowu et al., 2021).
748 Strong performance in 2015 indicates improved representation of atmospheric demand and
749 surface conductance dynamics during wet conditions, whereas larger dispersion and PBIAS in
750 2008 (RMSE: 2.05 Kg H_2O m^{-2} day^{-1}; PBIAS: -36.0%) suggest sensitivity to seasonal
751 variations in soil moisture availability and evaporative demand. In contrast, WUE showed
752 comparatively better performance (R^2 of 0.38 to 0.78), consistent with the propagation of
753 uncertainties from both GPP and ET simulations. As WUE sensitive with the changes in ET,
754 and this sensitivity is clearly evident in 2015, where minor deviations in ET resulted in
755 disproportionately larger fluctuations (RMSE: 0.70 gC Kg^{-1} H_2O; PBIAS: -12.9%) in WUE.
756 Despite this, the model adequately captured the overall magnitude and interannual variability
757 of WUE, with RMSE lower than 0.75 gC kg^{-1} H_2O. Overall, the calibrated ISBA-A-g_s
758 framework effectively represents coupled carbon-water processes at the ecosystem scale,

https://doi.org/10.5194/egusphere-2026-3119
Preprint. Discussion started: 16 June 2026

demonstrating strongest performance for GPP and comparatively moderate uncertainty for WUE.

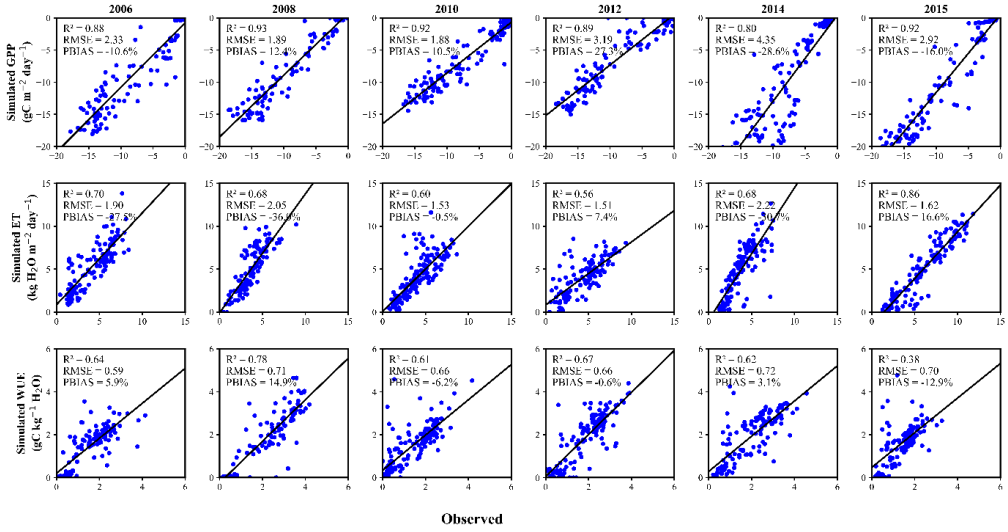

Figure 6. Scatter plots comparing daily eddy covariance observations with ISBA-A-g_s simulated gross primary productivity (GPP: first row), evapotranspiration (ET: second row), and water use efficiency (WUE: third row) at the FR-Lam site during six maize growing seasons (2006, 2008, 2010, 2012, 2014, and 2015). Statistical performance metrics, including the coefficient of determination (R^2), root mean square error (RMSE), and percentage bias (PBIAS), are reported in each panel.

The cumulative observed and simulated flux dynamics reveal pronounced interannual variability in seasonal GPP and ET at the FR-Lam site (Figure 7). Cumulative GPP ranged from -900 to -1500 gC m^{-2}, with the highest uptake observed in 2014 and 2015, and comparatively lower values in 2006 and 2008. The rapid slope in cumulative GPP during the peak growth phase (May-August) reflects intensified canopy photosynthesis, corresponding to maximum leaf area development. Quantitatively, the mean seasonal GPP accumulation rates (slope of cumulative curves) varied from -7.92 to -11.16 gC m^{-2} day^{-1} for observations and -6.87 to -12.91 gC m^{-2} day^{-1} for simulations, with higher values during 2015 (observed: -11.61; simulated: -12.10 gC m^{-2} day^{-1}) and lower values during 2008 (observed: -9.11; simulated: -

https://doi.org/10.5194/egusphere-2026-3119
Preprint. Discussion started: 16 June 2026

787 8.07 gC m^{-2} day^{-1}). Simulated cumulative GPP closely tracked observations in most years,
788 although noticeable overestimation occurred in 2014 and 2015. Cumulative ET varied between
789 500 and 800 kg H_2O m^{-2} across seasons, with wet years (e.g. 2014 and 2015) exhibiting greater
790 total water loss than dry years (e.g. 2006 and 2008). The steepest accumulation rates were
791 observed during mid-season (May-September). The seasonal ET accumulation rates ranged
792 from 3.860 to 6.730 kg H_2O m^{-2} day^{-1} (observed) and 4.075 to 5.768 kg H_2O m^{-2} day^{-1}
793 (simulated), with higher values during 2015 (observed: 6.73; Simulated: 5.76 kg H_2O m^{-2} day^{-1}) and lower values in 2008 (observed: 3.80; Simulated: 4.19 kg H_2O m^{-2} day^{-1}). While the
795 model reproduced the seasonal trajectory of ET, deviations in total seasonal ET were evident
796 in 2008 and 2014, suggesting model dependency on atmospheric dryness. Seasonal observed
797 WUE ranged from 1.60 to 2.22 g C kg^{-1} H_2O, while simulated values ranged from 1.37 to 2.21
798 g C kg^{-1} H_2O, reflecting the integrated balance between carbon gain and water loss. Years
799 characterized by lower evapotranspiration (e.g., 2008) exhibited higher WUE (observed: 2.22
800 g C kg^{-1} H_2O; simulated: 1.50 g C kg^{-1} H_2O), whereas seasons with relatively higher ET (e.g.,
801 2015) resulted in reduced WUE (observed: 1.60 g C kg^{-1} H_2O; simulated: 1.80 g C kg^{-1} H_2O).
802 Overall, the close agreement between simulated and observed values across seasons indicates
803 that the calibrated ISBA-A-g_s model effectively captures both daily variability and seasonal-
804 scale carbon-water dynamics, with only minor discrepancies.

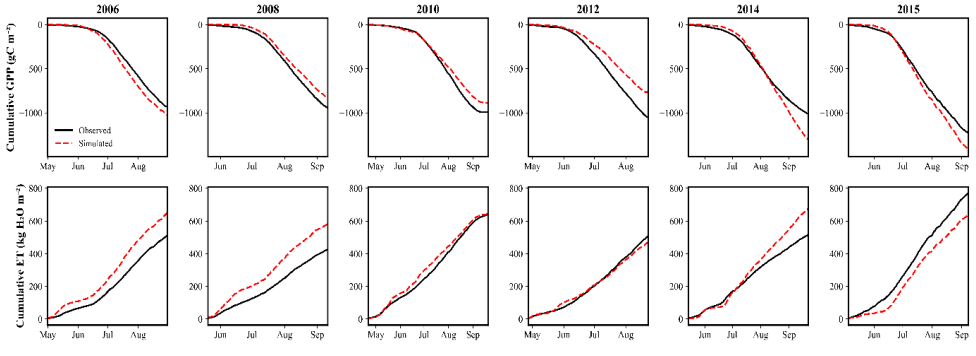

https://doi.org/10.5194/egusphere-2026-3119
Preprint. Discussion started: 16 June 2026

Figure 7. Cumulative plots by accumulating daily eddy covariance observations with ISBA-A-g_s simulated gross primary productivity (GPP: first row) and evapotranspiration (ET: second row) at the FR-Lam site during six maize growing seasons (2006, 2008, 2010, 2012, 2014, and 2015).

3.5 Model performance over the Ind-IITH site

The calibrated ISBA-A-g_s model showed robust performance in simulating GPP, ET, and WUE across irrigation treatments and seasons at the Ind-IITH site (Figure 8). For GPP, model performance was consistently strong, with R^2 ranging from 0.66 under AFI-Monsoon to 0.86 under AFI-Winter. In the CFI-Monsoon, GPP was reproduced with high accuracy (R^2 = 0.83; RMSE = 1.82 gC m^{-2} day^{-1}; PBIAS = 8.24%), indicating a slight underestimation of carbon uptake. Under AFI-Monsoon, performance decreased moderately (R^2 = 0.66; RMSE = 2.08 gC m^{-2} day^{-1}), although bias was minimal (PBIAS = -1.26%). During winter, model performance improved further, particularly under AFI (R^2 = 0.86; RMSE = 1.86 gC m^{-2} day^{-1}), although a systematic overestimation of GPP was observed (PBIAS = -20.25%). These results suggest that the model effectively captures seasonal photosynthetic dynamics, with slightly higher uncertainty under AFI during monsoon conditions due to the dominant influence of precipitation over irrigation inputs. ET simulations showed moderate agreement across treatments, with R^2 ranges between 0.51 and 0.61 during winter and between 0.53 and 0.55 during monsoon. In CFI-Monsoon, ET was simulated moderately (R^2 = 0.55; RMSE = 1.41 kg H_2O m^{-2} day^{-1}; PBIAS = 4.38%), indicating minor underestimation. Under AFI-Monsoon, bias shifted negative (PBIAS = -13.56%), suggesting overestimation of ET. Winter performance remained comparable (R^2 of 0.61 for CFI and 0.51 for AFI), although AFI-Winter exhibited larger overestimation (PBIAS = -18.76%). The relatively low R^2 values for ET compared to GPP reflect the stronger sensitivity of water fluxes to short-term meteorological variability and soil moisture dynamics, and higher heterogeneity for AFI treatment. WUE exhibited comparatively moderate performance, with R^2 ranging from 0.54 to 0.63. Under CFI-Monsoon,

https://doi.org/10.5194/egusphere-2026-3119
Preprint. Discussion started: 16 June 2026

WUE was simulated strongly, indicating better agreement and minimal bias (R^2 = 0.62; RMSE = 0.44 gC kg^{-1} H_2O; PBIAS = 2.10%). AFI-Monsoon showed similar performance (R^2 = 0.63; RMSE = 0.58 gC kg^{-1} H_2O), although with moderate underestimation (PBIAS = 6.03%). During winter, WUE performance remained consistent (R^2 = 0.60 for CFI and 0.54 for AFI), with bias ranging from -7.40% to 14.90%. The comparatively lower R^2 for WUE reflects the propagation of uncertainties from both GPP and ET simulations, as small deviations in ET can induce amplified variability in WUE simulations. Overall, model performance was strongest for GPP, moderate for ET, and WUE simulations. Seasonal contrasts indicate that the ISBA-A-g_s model captures GPP more robustly than ET and WUE fluxes, while AFI introduces slightly higher variability in both ET and WUE simulations.

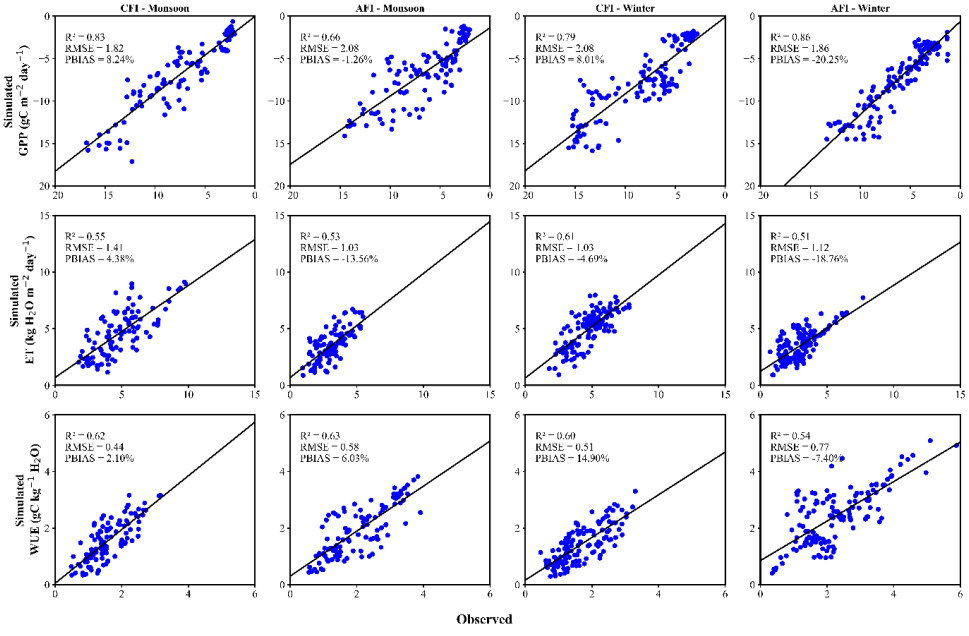

Figure 8. Scatter plots comparing daily eddy covariance observations with ISBA-A-g_s simulated gross primary productivity (GPP: first row), evapotranspiration (ET: second row), and water use efficiency (WUE: third row) at the Ind-IITH site during four maize treatments considered. Statistical performance metrics, including the coefficient of determination (R^2), root mean square error (RMSE), and percentage bias (PBIAS), are reported in each panel.

https://doi.org/10.5194/egusphere-2026-3119
Preprint. Discussion started: 16 June 2026

The cumulative seasonal patterns reveal clear contrasts in GPP and ET between irrigation treatments and crop seasons at the Ind-IITH site (Figure 9). During the monsoon, cumulative GPP reached to -820 gC m^{-2} under CFI and -780 gC m^{-2} under AFI. The corresponding seasonal GPP accumulation rates (slope of cumulative curves) were -8.90 and -7.82 gC m^{-2} day^{-1} for observed CFI and AFI, respectively, with simulated values of -8.21 and -7.68 gC m^{-2} day^{-1}. The close agreement between observed and simulated trajectories indicates that the model adequately captured seasonal carbon assimilation under monsoon conditions, although simulated GPP slightly overestimated during late-season phases in both treatments. In contrast, winter season GPP accumulation was substantially higher, reaching nearly -1050 gC m^{-2} under CFI and approximately -900 gC m^{-2} under AFI. The steeper mid-season slope (Jan-Mar) reflects enhanced radiation availability and sustained canopy activity during winter. Quantitatively, GPP accumulation rates were -8.89 and -6.94 gC m^{-2} day^{-1} for observed CFI and AFI, respectively, compared to -8.04 and -8.32 gC m^{-2} day^{-1} for simulations, indicating a tendency of the model to overestimate carbon uptake under AFI-Winter, particularly during the late reproductive stage. These results indicate that winter conditions favoured greater seasonal carbon assimilation compared to monsoon, likely due to reduced cloud cover and more stable atmospheric demand. During the monsoon, total ET reached to 500 kg H_2O m^{-2} for CFI and around 380 kg H_2O m^{-2} for AFI. The reduced ET under AFI reflects lower water inputs and moderated transpiration rates. The seasonal ET accumulation rates were 4.97 and 3.25 kg H_2O m^{-2} day^{-1} for observed CFI and AFI, respectively, against simulated values of 4.66 and 3.74 kg H_2O m^{-2} day^{-1}. Simulated ET closely tracked observed patterns in CFI-Monsoon, whereas slight overestimation was evident in AFI-Monsoon during mid-season. Winter ET was substantially higher, reaching to 650 kg H_2O m^{-2} under CFI and 450 kg H_2O m^{-2} under AFI. The corresponding ET accumulation rates were 4.80 and 3.02 kg H_2O m^{-2} day^{-1} for observed

https://doi.org/10.5194/egusphere-2026-3119
Preprint. Discussion started: 16 June 2026

CFI and AFI, compared to 5.10 and 3.68 kg H_2O m^{-2} day^{-1} for simulations. The larger seasonal ET under winter suggests stronger evaporative demand. Notably, the divergence between CFI and AFI was more pronounced during winter, indicating enhanced sensitivity of transpiration to irrigation management under drier atmospheric conditions. These relatively temperate-like conditions, characterized by lower humidity and higher evaporative demand, tend to amplify the differences between irrigation methods, where CFI promotes higher soil moisture availability and transpiration, while AFI regulates water supply and limits excessive evaporative losses. During the monsoon season, observed WUE was 1.55 g C kg^{-1} H_2O under CFI and 1.61 g C kg^{-1} H_2O under AFI, while the corresponding simulated values were 1.54 and 1.86 g C kg^{-1} H_2O, respectively. The higher WUE under AFI indicates enhanced carbon gain per unit water consumed, likely driven by partial stomatal regulation and more conservative water use under alternate irrigation practices. In winter, observed WUE increased further, reaching 1.67 g C kg^{-1} H_2O under CFI and approximately 1.82 g C kg^{-1} H_2O under AFI, whereas simulated values were 1.46 and 2.13 g C kg^{-1} H_2O, respectively. Overall, the model successfully captured the seasonal WUE, although minor deviations were observed during the late-season period, particularly under AFI conditions in winter.

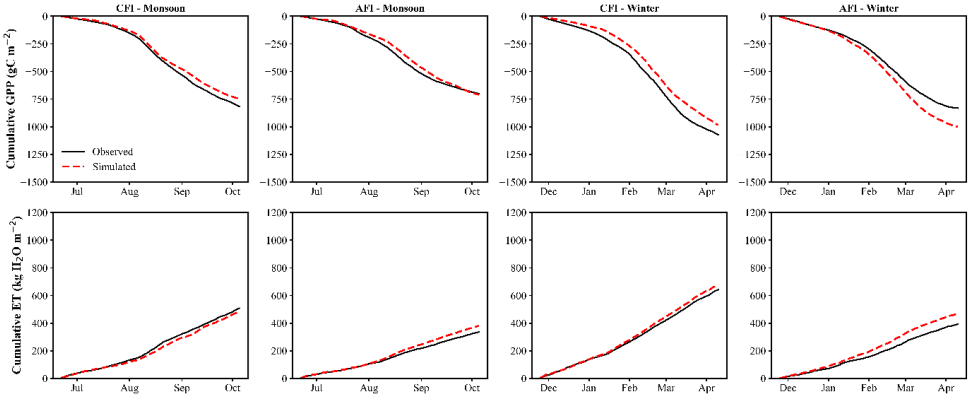

https://doi.org/10.5194/egusphere-2026-3119
Preprint. Discussion started: 16 June 2026

Figure 9. Cumulative plots by accumulating daily eddy covariance observations with ISBA-A-g_s simulated gross primary productivity (GPP: first row) and evapotranspiration (ET: second row) at the Ind-IITH site for four maize treatments considered.

3.6 Model assessment

Figure 10 illustrates the variability in the slope of the GPP.VPD$^{0.5}$ - ET relationship at both FR-Lam and Ind-IITH sites. This slope represents an ecosystem-scale coupling between carbon assimilation and evapotranspiration. A higher slope indicates more efficient carbon gain per unit water loss, associated with stronger stomatal regulation, whereas a lower slope suggests increased water loss relative to carbon uptake and reduced efficiency. At FR-Lam, observed slopes ranged from -10.15 to -14.44 gC hPa$^{0.5}$ kg^{-1} H_2O. The strongest atmospheric sensitivity was observed in 2008 (-14.44 gC hPa$^{0.5}$ kg^{-1} H_2O), whereas comparatively weaker sensitivity occurred in 2014 (-10.15 gC hPa$^{0.5}$ kg^{-1} H_2O). The ISBA-A-g_s simulations closely reproduced the interannual variability, with simulated slopes differing marginally (within ± 0.36 gC hPa$^{0.5}$ kg^{-1} H_2O) from observations. Slight underestimation of slope magnitude was evident in 2006 and 2012, whereas 2014 showed a small overestimation. Overall, ISBA-A-g_s successfully captured the coupling between carbon assimilation and atmospheric demand during peak canopy development. At Ind-IITH, slope magnitudes were generally stronger than those observed at FR-Lam, particularly during the winter season. Under CFI-Monsoon conditions, the observed slope was recorded as -12.92 gC hPa$^{0.5}$ kg^{-1} H_2O, while AFI-Monsoon exhibited a stronger response (-13.85 gC hPa$^{0.5}$ kg^{-1} H_2O), suggesting enhanced atmospheric control under AFI. During winter, the slopes intensified further, reached to -15.28 gC hPa$^{0.5}$ kg^{-1} H_2O under AFI. The ISBA-A-g_s simulations reproduced these seasonal and treatment contrasts (within ± 0.74 gC hPa$^{0.5}$ kg^{-1} H_2O), although a slight underestimation of magnitude was observed under AFI. Comparatively, the stronger slopes at Ind-IITH indicate a greater sensitivity of carbon-water coupling to atmospheric demand in the semi-arid tropical

https://doi.org/10.5194/egusphere-2026-3119
Preprint. Discussion started: 16 June 2026

environment relative to the temperate FR-Lam site. Overall, the close agreement between observed and simulated slopes across both sites demonstrates the robustness of ISBA-A-g_s in representing the atmospheric regulation of carbon-water interactions under contrasting hydro-climatic regimes.

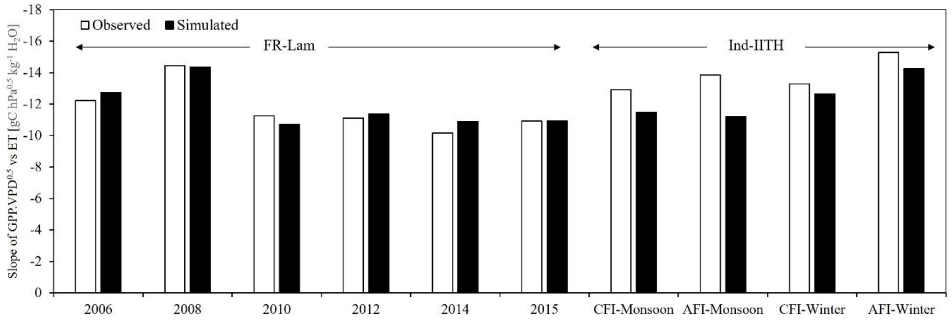

Figure 10. Seasonal variability in the slope of the GPP.VPD$^{0.5}$ versus ET relationship at the FR-Lam and Ind-IITH sites. Solid bars represent observed EC estimates, while hatched bars denote ISBA-A-g_s simulated values.

Figure 11 shows the slope of the evaporative fraction (EF)-VPD relationship at both FR-Lam and Ind-IITH sites. This relationship reflects the ecosystem-scale response of surface energy partitioning to atmospheric demand and provides indirect insight into land-atmosphere coupling and stomatal regulation. A steeper slope suggests a stronger sensitivity of latent heat flux to VPD, indicating tighter stomatal or moisture control, whereas a weaker slope may reflect reduced coupling or increased non-stomatal limitations. At FR-Lam, observed slopes ranged from 0.0014 (2008) to 0.0086 (2015), reflecting substantial interannual variability in surface energy partitioning. Moderate slopes were recorded in 2006 (0.0043) and 2012 (0.0046), while enhanced coupling between EF and VPD was evident in 2014 (0.0072) and 2015 (0.0086). The interannual range (0.0072) highlights marked differences in surface moisture availability and evaporative dominance across years. ISBA-A-g_s simulations closely reproduced this variability, with simulated slopes ranging between 0.0012 and 0.0085, and

https://doi.org/10.5194/egusphere-2026-3119
Preprint. Discussion started: 16 June 2026

deviations within ± 0.001-0.0015. At Ind-IITH, clear irrigation and seasonal contrasts were observed. Under CFI-Monsoon, the observed slope was 0.0061, whereas under AFI-Monsoon, it decreased markedly to 0.0021, indicating a nearly 65% reduction in EF sensitivity under AFI. A similar contrast was evident during winter, where slopes were 0.0069 under CFI-Winter and only 0.0025 under AFI-Winter, representing a reduction of approximately 60-65% under AFI. These results indicate that CFI enhances the responsiveness of evaporative fraction to increases in VPD, while partial soil wetting under AFI dampens this response. ISBA-A-g_s successfully captured both the magnitude and direction of these treatment-induced contrasts, although slight underestimation occurred under winter CFI conditions (0.001 difference). Overall, the positive EF-VPD slopes confirm that VPD dominates surface energy partitioning during peak LAI periods. Higher slopes at FR-Lam during 2014-2015 and under CFI treatments at Ind-IITH reflect moisture-sufficient conditions promoting strong coupling between carbon assimilation and evapotranspiration. At FR-Lam, these elevated slopes may also be partly attributed to the change in maize cultivar during 2014-2015, which resulted in enhanced canopy development and higher LAI, thereby influencing ecosystem-scale fluxes. In contrast, reduced slopes under AFI indicate moderated evaporative response due to partial soil drying and regulated surface moisture availability.

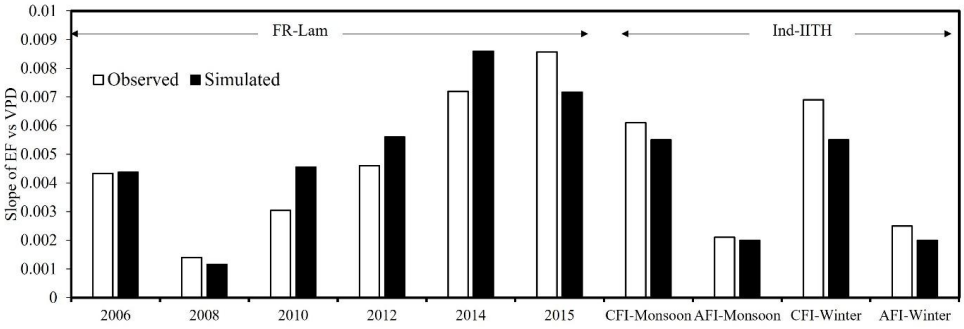

Figure 11. Variability in the slope of the EF vs VPD relationship at the FR-Lam and Ind-IITH sites. Solid bars represent observed EC estimates, and hatched bars denote ISBA-A-g_s simulated values.

https://doi.org/10.5194/egusphere-2026-3119
Preprint. Discussion started: 16 June 2026

4.0 Discussions

The calibrated ISBA-A-g_s framework demonstrated robust performance in reproducing the magnitude, variability, and seasonal progression of GPP, ET, and WUE at both the FR-Lam and Ind-IITH sites, confirming its ability to represent coupled carbon-water processes across contrasting hydro-climatic regimes. The consistently higher performance for GPP compared to ET aligns with previous evaluations of land surface models, where photosynthetic parameterization is often more constrained than evapotranspiration processes that depend on soil moisture dynamics and surface conductance variability (Best et al., 2011; Bonan et al., 2011). The strong GPP simulations (Figure 6 and 7) across both wet and dry years at FR-Lam suggest that the Jacob's-based photosynthesis scheme within ISBA-A-g_s effectively captures biochemical limitations and radiation-driven assimilation across moisture gradients. However, relatively moderate uncertainties in ET, particularly during years with irregular precipitation distribution (e.g. 2012), indicate sensitivity to soil water stress parameterization and aerodynamic coupling, consistent with findings reported by (Dare-Idowu et al., 2021; De Kauwe et al., 2013; Seneviratne et al., 2010). As WUE integrates both carbon gain and water loss, its variability amplifies with small deviations in ET, explaining the comparatively lower R^2 values (Figure 6) observed for WUE during wet years (2014 and 2015). Similar propagation effects have been reported in cropland ecosystems, where ET biases disproportionately affect WUE simulations (Medlyn et al., 2011; Zhou et al., 2014). The pronounced interannual variability in cumulative GPP (-950 to -1400 g C m^{-2}) and ET (800 - 1150 kg H_2O m^{-2}) at FR-Lam reflects strong climatic regulation of seasonal carbon-water budgets, but also includes cultivar effects (Figure 7). This behaviour is consistent with observations from temperate croplands showing positive GPP anomalies during moist growing seasons (Ciais et al., 2005; Reichstein et al., 2013). Interestingly, increased ET in wet years did not proportionally enhance

https://doi.org/10.5194/egusphere-2026-3119
Preprint. Discussion started: 16 June 2026

WUE, indicating that additional water availability stimulated transpiration more strongly than carbon assimilation. Such decoupling between GPP and ET under high evaporative demand has been observed in maize systems where stomatal regulation becomes increasingly responsive to atmospheric VPD rather than soil moisture alone (Kang et al., 2001; Tardieu et al., 2015). The performance of ISBA-A-g_s to reproduce these cumulative trajectories suggests that the model captures seasonal-scale feedbacks between canopy development and atmospheric demand (Figure 7 and 9). At the semi-arid Ind-IITH site, irrigation management introduced an additional layer of control over carbon-water dynamics. The higher cumulative GPP during winter compared to monsoon reflects improved radiation availability and lower cloud cover, which enhanced photosynthetic efficiency despite higher evaporative demand (Figure 9). Similar seasonal contrasts have been reported for tropical and subtropical maize systems, where winter cropping benefits from stable radiation regimes and reduced atmospheric variability (Deb Burman et al., 2024; Lobell et al., 2011). The reduced ET under AFI relative to CFI, particularly during monsoon, indicates partial stomatal regulation and moderated transpiration without proportionally reducing carbon assimilation (Fereres and Soriano, 2007; Kang et al., 2001). Consequently, average WUE was consistently higher under AFI, as observed in previous studies of (Geerts and Raes, 2009; Medrano et al., 2015). ISBA-A-g_s ability to capture this treatment-specific divergence highlights the robustness of its soil moisture stress formulation and canopy resistance parameterization (Figure 8 and 9).

The diagnostic analyses using GPP·$VPD^{0.5}$-ET relationships and EF-VPD responses further demonstrate that the model captures underlying eco-physiological controls beyond statistical agreement (Figure 10). The normalization of GPP by VPD effectively isolates biochemical limitations from atmospheric demand effects (Zhou et al., 2014), so it focuses on plant physiology and should be similar according to the same plant cultivar. So the EF sensitivity to VPD reflects surface energy partitioning regulated by stomatal conductance and

https://doi.org/10.5194/egusphere-2026-3119
Preprint. Discussion started: 16 June 2026

soil moisture availability (Seneviratne et al., 2010). Across both sites, steeper cumulative slopes during peak canopy development confirm that LAI-mediated increases in photosynthetic capacity drive mid-season carbon assimilation. The consistency between simulated and observed cumulative patterns suggests that ISBA-A-g_s realistically represents canopy phenology-hydrology interactions, a key requirement for predicting future carbon-water feedbacks under climate variability. Overall, the stronger performance for GPP relative to ET and WUE suggests that while biochemical assimilation processes are well constrained, hydrological components remain more sensitive to meteorological forcing. Given the increasing importance of optimizing irrigation under climate change, accurate representation of ET partitioning and stomatal regulation is critical for reliable WUE projections. The demonstrated capability of ISBA-A-g_s to reproduce interannual variability in ET and soil moisture contrasts, and cumulative seasonal budgets across temperate (FR-Lam) and tropical semi-arid (Ind-IITH) agro-ecosystems indicates strong potential for its application in climate-resilient water resources planning and carbon-water management strategies.

5.0 Model limitations and Future scope

In the current configuration, LAI was prescribed at 10-day intervals. Such temporal aggregation may be insufficient for fast-growing crops like maize, where rapid phenological development and canopy expansion occur within shorter timescales (< 10 days). Consequently, micro-physiological responses and short-term canopy dynamics may be masked within these averaged inputs, potentially contributing to the observed overestimation of fluxes during peak growth stages. Further, the model calibration was performed using a “one-at-a-time” parameter optimization approach. While computationally efficient, this method neglects potential interactive and nonlinear effects among parameters. Finally, the seasonal climatic variability posed a significant challenge for parameter transferability. Contrasting hydro-climatic

https://doi.org/10.5194/egusphere-2026-3119
Preprint. Discussion started: 16 June 2026

conditions across maize growing seasons (monsoon vs. winter in India; wet vs. dry seasons in France) influence radiation regimes, VPD dynamics, and soil moisture availability. These variations propagate uncertainty during calibration and may partly explain mismatches between observed and simulated datasets.

This study represents the first application of a locally calibrated ISBA model in its MEB configuration to simulate GPP, ET, and WUE of maize in a tropical semi-arid Indian agro-ecosystem. Since WUE is a critical eco-hydrological indicator, this study advances the quantitative understanding of WUE variability under contrasting hydro-climatic conditions and irrigation regimes. The successful adaptation and validation of the ISBA-A-g_s model establishes a robust foundation for process-based agro-hydrological assessments. The calibrated model can be further utilized to detect water stress conditions to investigate the response of evapotranspiration to varying climatic demand. Future, incorporating higher temporal resolution vegetation dynamics (e.g., LAI and phenology updates at sub-weekly scales), employing multi-parameter or global optimization techniques (e.g., Monte Carlo, Bayesian calibration) to capture nonlinear parameter interactions can further improve the model accuracy. Further, the expanding simulations across multiple growing seasons and diverse irrigation/management scenarios to enhance model robustness.

6.0 Conclusions

This study aimed to investigate ecosystem-scale GPP, ET, and WUE dynamics of maize grown under two contrasting hydro-climatic conditions: temperate (FR-Lam, France) and tropical semi-arid (Ind-IITH, India), using the ISBA-A-g_s SVAT model within the SURFEX land surface modelling framework. The model was driven by in-situ meteorological measurements, along with observed vegetation variables, and was subsequently calibrated and

https://doi.org/10.5194/egusphere-2026-3119
Preprint. Discussion started: 16 June 2026

validated to simulate seasonal variations in GPP, ET, and WUE. The key findings of this study are summarized as follows:

1. This study presents the first application of the MEB configuration of the ISBA-A-g_s land surface model to quantify ecosystem-scale GPP, ET, and WUE dynamics in both temperate (FR-Lam) and semi-arid Indian (Ind-IITH) agro-ecosystems, addressing a critical observational and modelling gap.
2. This study provides site-specific calibrated biogeochemical parameters for maize in semi-arid India, offering a robust foundation for improved regional-scale simulations of carbon-water interactions and WUE dynamics.
3. The calibrated ISBA-A-g_s model reliably reproduced ecosystem-scale GPP and ET fluxes under both temperate (FR-Lam) and tropical semi-arid (Ind-IITH) conditions, demonstrating strong transferability across contrasting hydro-climatic regimes.
4. At the FR-Lam site, GPP was simulated with high accuracy (R^2 of 0.80 to 0.93), whereas ET and WUE showed greater sensitivity to meteorological variability, emphasizing the inherent complexity and atmospheric dependence of hydrological processes.
5. At the Ind-IITH site, ISBA-A-g_s consistently reproduced GPP more robustly, followed by ET and WUE, with AFI treatment introducing additional variability in simulated ET fluxes. The model's ability to resolve irrigation-specific divergence between CFI and AFI treatments underscores the strength of its soil moisture stress representation and canopy resistance parameterization.
6. ISBA-A-g_s effectively captured both interannual variability and irrigation-induced contrasts, with simulated GPP·$VPD^{0.5}$-ET slopes closely aligning with observations (within ± 0.36 gC $hPa^{0.5}$ kg^{-1} H_2O (FR-Lam) and ± 0.74 gC $hPa^{0.5}$ kg^{-1} H_2O (Ind-IITH)), confirming its ability to represent atmospheric regulation of carbon-water coupling.

https://doi.org/10.5194/egusphere-2026-3119
Preprint. Discussion started: 16 June 2026

The demonstrated ability of the ISBA-A-g_s model to reproduce interannual variability, irrigation effects, and cumulative seasonal carbon-water budgets across temperate (FR-Lam) and tropical semi-arid (Ind-IITH) agro-ecosystems underscores its strong potential for application in climate-resilient irrigation management and carbon-water optimization strategies.

Acknowledgements

The corresponding author thanks CEFIPRA for facilitating a research mobility to CESBIO, Toulouse, France, through the Raman Charpak Fellowship. The corresponding author also acknowledges the financial support provided by the Ministry of Education, Government of India, through the Prime Minister's Research Fellowship (PMRF) for the Grant Number PMRF/2002195. The authors acknowledge undergraduate students of the College of Agriculture Engineering, Sangareddy, for helping during field experiments in India. Data acquisition for FR-Lam was funded by the Institut National des Sciences de l'Univers of the Centre National de la Recherche Scientifique through ICOS. Facilities and staff were also funded by the University of Paul Sabatier, CNES, and Institut de Recherche pour le Développement.

Credit authorship contribution statement

Syam Chintala: Experimentation, Data collection and curation, Methodology, Model setup simulations, Results Analysis, Investigation, Writing - Original draft. **Lionel Jarlan:** Results analysis, Writing - Original draft & editing, Project administration, Supervision. **Vincent Rivalland:** Results Analysis and interpretation, and Writing - Original draft & review. **Aaron Boone:** Results analysis and Model setup. **Oluwakemi Dare-Idowu:** Data curation and Input data preparation. **Valerie Le Dantec:** Results interpretation and Writing - Original draft &

https://doi.org/10.5194/egusphere-2026-3119
Preprint. Discussion started: 16 June 2026

review. **Gilles Boulet**: Results interpretation and Writing - Original draft & review. **BVN P Kambhammettu**: Results analysis, Writing - Original draft & review, Project administration, Supervision. **Aurore Brut**: Results analysis, Writing - Original draft & review, Project administration, Supervision.

Code/Data availability statement

Relevant Codes and Data will be made available on request.

Declaration of Competing Interest

The authors declare that they have no known competing financial interests or personal relationships that could have appeared to influence the work reported in this paper.

References

Al-Kayssi, A. A.: Role of alternate and fixed partial root-zone drying on water use efficiency and growth of maize (Zea mays L.) in gypsiferous soils, International Soil and Water Conservation Research, 11, 145–158, https://doi.org/10.1016/j.iswcr.2022.04.003, 2023.

Aouade, G., Jarlan, L., Ezzahar, J., Er-Raki, S., Napoly, A., Benkaddour, A., Khabba, S., Boulet, G., Garrigues, S., and Chehbouni, A.: Evapotranspiration partition using the multiple energy balance version of the ISBA-Ag s land surface model over two irrigated crops in a semi-arid Mediterranean region (Marrakech, Morocco), Hydrol. Earth Syst. Sci., 24, 3789–3814, 2020.

Aubinet, M., Grelle, A., Ibrom, A., Rannik, Ü., Moncrieff, J., Foken, T., Kowalski, A. S., Martin, P. H., Berbigier, P., and Bernhofer, C.: Estimates of the annual net carbon and water exchange of forests: the EUROFLUX methodology, in: Advances in ecological research, vol. 30, Elsevier, 113–175, 1999.

https://doi.org/10.5194/egusphere-2026-3119
Preprint. Discussion started: 16 June 2026

1168 Baldocchi, D.: Measuring fluxes of trace gases and energy between ecosystems and the
1169 atmosphere – the state and future of the eddy covariance method, Glob. Chang. Biol., 20,
1170 3600–3609, https://doi.org/https://doi.org/10.1111/gcb.12649, 2014.

1171 Baldocchi, D., Falge, E., Gu, L., Olson, R., Hollinger, D., Running, S., Anthoni, P., Bernhofer,
1172 Ch., Davis, K., Evans, R., Fuentes, J., Goldstein, A., Katul, G., Law, B., Lee, X., Malhi, Y.,
1173 Meyers, T., Munger, W., Oechel, W., U, K. T. P., Pilegaard, K., Schmid, H. P., Valentini, R.,
1174 Verma, S., Vesala, T., Wilson, K., and Wofsy, S.: FLUXNET: A New Tool to Study the
1175 Temporal and Spatial Variability of Ecosystem-Scale Carbon Dioxide, Water Vapor, and
1176 Energy Flux Densities, Bull. Am. Meteorol. Soc., 82, 2415–2434,
1177 https://doi.org/10.1175/1520-0477(2001)082<2415:FANTTS>2.3.CO;2, 2001.

1178 Barr, A. G., Morgenstern, K., Black, T. A., McCaughey, J. H., and Nesic, Z.: Surface energy
1179 balance closure by the eddy-covariance method above three boreal forest stands and
1180 implications for the measurement of the CO2 flux, Agric. For. Meteorol., 140, 322–337,
1181 https://doi.org/10.1016/j.agrformet.2006.08.007, 2006.

1182 Battude, M., Al Bitar, A., Brut, A., Tallec, T., Huc, M., Cros, J., Weber, J.-J., Lhuissier, L.,
1183 Simonneaux, V., and Demarez, V.: Modeling water needs and total irrigation depths of maize
1184 crop in the south west of France using high spatial and temporal resolution satellite imagery,
1185 Agric. Water Manag., 189, 123–136, 2017.

1186 Beer, C., Ciais, P., Reichstein, M., Baldocchi, D., Law, B. E., Papale, D., Soussana, J. F.,
1187 Ammann, C., Buchmann, N., Frank, D., Gianelle, D., Janssens, I. A., Knohl, A., Köstner,
1188 B., Moors, E., Roupsard, O., Verbeeck, H., Vesala, T., Williams, C. A., and Wohlfahrt, G.:
1189 Temporal and among-site variability of inherent water use efficiency at the ecosystem level,
1190 Global Biogeochem. Cycles, 23, 1–13, https://doi.org/10.1029/2008GB003233, 2009.

https://doi.org/10.5194/egusphere-2026-3119
Preprint. Discussion started: 16 June 2026

1191 Beer, C., Reichstein, M., Tomelleri, E., Ciais, P., Jung, M., Carvalhais, N., Rödenbeck, C.,
1192 Arain, M. A., Baldocchi, D., Bonan, G. B., Bondeau, A., Cescatti, A., Lasslop, G., Lindroth,
1193 A., Lomas, M., Luyssaert, S., Margolis, H., Oleson, K. W., Roupsard, O., Veenendaal, E.,
1194 Viovy, N., Williams, C., Woodward, F. I., and Papale, D.: Terrestrial Gross Carbon Dioxide
1195 Uptake: Global Distribution and Covariation with Climate, Science (1979)., 329, 834–838,
1196 https://doi.org/10.1126/science.1184984, 2010.

1197 Best, M. J., Pryor, M., Clark, D. B., Rooney, G. G., Essery, R. L. H., Menard, C. B., Edwards,
1198 J. M., Hendry, M. A., Porson, A., and Gedney, N.: The Joint UK Land Environment
1199 Simulator (JULES), model description–Part 1: energy and water fluxes, Geosci. Model
1200 Dev., 4, 677–699, 2011.

1201 Béziat, P., Rivalland, V., Jarosz, N., Ceschia, E., Boulet, G., and Gentine, P.: Crop
1202 evapotranspiration partitioning and comparison of different water use efficiency
1203 approaches, in: EGU General Assembly Conference Abstracts, 3394, 2010.

1204 Bonan, G. B., Lawrence, P. J., Oleson, K. W., Levis, S., Jung, M., Reichstein, M., Lawrence,
1205 D. M., and Swenson, S. C.: Improving canopy processes in the Community Land Model
1206 version 4 (CLM4) using global flux fields empirically inferred from FLUXNET data, J.
1207 Geophys. Res. Biogeosci., 116, 2011.

1208 Boone, A., Samuelsson, P., Gollvik, S., Napoly, A., Jarlan, L., Brun, E., and Decharme, B.: The
1209 interactions between soil–biosphere–atmosphere land surface model with a multi-energy
1210 balance (ISBA-MEB) option in SURFEXv8–Part 1: Model description, Geosci. Model
1211 Dev., 10, 843–872, 2017.

1212 Buckley, T. N.: Modeling stomatal conductance, Plant Physiol., 174, 572–582, 2017.

https://doi.org/10.5194/egusphere-2026-3119
Preprint. Discussion started: 16 June 2026

1213 Calvet, J.-C.: Investigating soil and atmospheric plant water stress using physiological and
1214 micrometeorological data, Agric. For. Meteorol., 103, 229–247,
1215 https://doi.org/https://doi.org/10.1016/S0168-1923(00)00130-1, 2000.

1216 Calvet, J.-C., Noilhan, J., Roujean, J.-L., Bessemoulin, P., Cabelguenne, M., Olioso, A., and
1217 Wigneron, J.-P.: An interactive vegetation SVAT model tested against data from six
1218 contrasting sites, Agric. For. Meteorol., 92, 73–95, 1998.

1219 Chen, Y., Ding, Z., Yu, P., Yang, H., Song, L., Fan, L., Han, X., Ma, M., and Tang, X.:
1220 Quantifying the variability in water use efficiency from the canopy to ecosystem scale across
1221 main croplands, Agric. Water Manag., 262, 107427,
1222 https://doi.org/10.1016/j.agwat.2021.107427, 2022.

1223 Ciais, P., Reichstein, M., Viovy, N., Granier, A., Ogée, J., Allard, V., Aubinet, M., Buchmann,
1224 N., Bernhofer, C., and Carrara, A.: Europe-wide reduction in primary productivity caused
1225 by the heat and drought in 2003, Nature, 437, 529–533, 2005.

1226 Claverie, M., Demarez, V., Duchemin, B., Hagolle, O., Ducrot, D., Marais-Sicre, C., Dejoux,
1227 J.-F., Huc, M., Keravec, P., and Béziat, P.: Maize and sunflower biomass estimation in
1228 southwest France using high spatial and temporal resolution remote sensing data, Remote
1229 Sens. Environ., 124, 844–857, 2012.

1230 Cosby, B. J., Hornberger, G. M., Clapp, R. B., and Ginn, T.: A statistical exploration of the
1231 relationships of soil moisture characteristics to the physical properties of soils, Water
1232 Resour. Res., 20, 682–690, 1984.

1233 Cowan, I. R. and GD, F.: Stomatal function in relation to leaf metabolism and environment.,
1234 1977.

https://doi.org/10.5194/egusphere-2026-3119
Preprint. Discussion started: 16 June 2026

1235 Dare-Idowu, O., Jarlan, L., Le-Dantec, V., Rivalland, V., Ceschia, E., Boone, A., and Brut, A.:
1236 Hydrological Functioning of Maize Crops in Southwest France Using Eddy Covariance
1237 Measurements and a Land Surface Model, Water (Basel)., 13,
1238 https://doi.org/10.3390/w13111481, 2021.

1239 Deb Burman, P. K., A.G., P., Chakraborty, S., Tiwari, Y. K., Sarma, D., and Gogoi, N.:
1240 Simulating the ecosystem-atmosphere carbon, water and energy fluxes at a subtropical
1241 Indian forest using an ecosystem model, Ecol. Modell., 490,
1242 https://doi.org/10.1016/j.ecolmodel.2024.110637, 2024.

1243 Decharme, B., Tzanos, D., Hardouin, L., Boone, A., Minvielle, M., and Le, P.: A process-based
1244 modeling of soil organic matter physical properties for land surface models - Part 2 : Global
1245 land surface simulations and mineral soil compaction adjustment, 1–54, 2026.

1246 Demarty, J., Ottlé, C., Braud, I., Olioso, A., Frangi, J. P., Gupta, H. V, and Bastidas, L. A.:
1247 Constraining a physically based soil-vegetation-atmosphere transfer model with surface
1248 water content and thermal infrared brightness temperature measurements using a
1249 multiobjective approach, Water Resour. Res., 41, 2005.

1250 Erenstein, O., Jaleta, M., Sonder, K., Mottaleb, K., and Prasanna, B. M.: Global maize
1251 production, consumption and trade: trends and R&D implications, Food Secur., 14, 1295–
1252 1319, https://doi.org/10.1007/s12571-022-01288-7, 2022.

1253 FAO: The future of food and agriculture: Trends and challenges, FAO, 2017.

1254 Faroux, S., Kaptué Tchuenté, A. T., Roujean, J.-L., Masson, V., Martin, E., and Le Moigne, P.:
1255 ECOCLIMAP-II/Europe: A twofold database of ecosystems and surface parameters at 1 km
1256 resolution based on satellite information for use in land surface, meteorological and climate
1257 models, Geosci. Model Dev., 6, 563–582, 2013.

https://doi.org/10.5194/egusphere-2026-3119
Preprint. Discussion started: 16 June 2026

1258 Fereres, E. and Soriano, M. A.: Deficit irrigation for reducing agricultural water use, J. Exp.
1259 Bot., 58, 147–159, 2007.

1260 Geerts, S. and Raes, D.: Deficit irrigation as an on-farm strategy to maximize crop water
1261 productivity in dry areas, Agric. Water Manag., 96, 1275–1284, 2009.

1262 Gibelin, A., Calvet, J., Roujean, J., Jarlan, L., and Los, S. O.: Ability of the land surface model
1263 ISBA-A-gs to simulate leaf area index at the global scale: Comparison with satellites
1264 products, Journal of Geophysical Research: Atmospheres, 111, 2006.

1265 Goetz, S. J., Baccini, A., Laporte, N. T., Johns, T., Walker, W., Kellndorfer, J., Houghton, R.
1266 A., and Sun, M.: Mapping and monitoring carbon stocks with satellite observations: a
1267 comparison of methods, Carbon Balance Manag., 4, 2, 2009.

1268 Hoover, D. L., Abendroth, L. J., Browning, D. M., Saha, A., Snyder, K., Wagle, P., Witthaus,
1269 L., Baffaut, C., Biederman, J. A., Bosch, D. D., Bracho, R., Busch, D., Clark, P., Ellsworth,
1270 P., Fay, P. A., Flerchinger, G., Kearney, S., Levers, L., Saliendra, N., Schmer, M.,
1271 Schomberg, H., and Scott, R. L.: Indicators of water use efficiency across diverse
1272 agroecosystems and spatiotemporal scales, Science of The Total Environment, 864, 160992,
1273 https://doi.org/https://doi.org/10.1016/j.scitotenv.2022.160992, 2023.

1274 Ito, A. and Inatomi, M.: Use of a process-based model for assessing the methane budgets of
1275 global terrestrial ecosystems and evaluation of uncertainty, Biogeosciences, 9, 759–773,
1276 https://doi.org/10.5194/bg-9-759-2012, 2012.

1277 Jacobs, C. M. J.: Direct impact of atmospheric CO2 enrichment on regional transpiration,
1278 Wageningen University and Research, 1994.

https://doi.org/10.5194/egusphere-2026-3119
Preprint. Discussion started: 16 June 2026

1279 Jacobs, C. M. J., Van den Hurk, B. M. M., and De Bruin, H. A. R.: Stomatal behaviour and
1280 photosynthetic rate of unstressed grapevines in semi-arid conditions, Agric. For. Meteorol.,
1281 80, 111–134, 1996.

1282 Jarvis, P.: The interpretation of the variations in leaf water potential and stomatal conductance
1283 found in canopies in the field, Philosophical Transactions of the Royal Society of London.
1284 B, Biological Sciences, 273, 593–610, 1976.

1285 Jung, M., Reichstein, M., Ciais, P., Seneviratne, S. I., Sheffield, J., Goulden, M. L., Bonan, G.,
1286 Cescatti, A., Chen, J., and De Jeu, R.: Recent decline in the global land evapotranspiration
1287 trend due to limited moisture supply, Nature, 467, 951–954, 2010.

1288 Kalma, J. D. and Stanhill, G.: The radiation climate of an irrigated orange plantation, Solar
1289 Energy, 12, 491–508, 1969.

1290 Kang, S., Liang, Z., Hu, W., and Zhang, J.: Water use efficiency of controlled alternate
1291 irrigation on root-divided maize plants, Agric. Water Manag., 38, 69–76,
1292 https://doi.org/10.1016/S0378-3774(98)00048-1, 1998.

1293 Kang, S., Zhang, L., Hu, X., Li, Z., and Jerie, P.: An improved water use efficiency for hot
1294 pepper grown under controlled alternate drip irrigation on partial roots, Sci. Hortic., 89,
1295 257–267, https://doi.org/10.1016/S0304-4238(00)00245-4, 2001.

1296 Karimindla, A. R., Kumari, S., S R, S., Chintala, S., and P. Kambhammettu, B.: The role of
1297 time averaging of eddy covariance fluxes on water use efficiency dynamics of maize, Atmos.
1298 Meas. Tech., 17, 5477–5490, https://doi.org/10.5194/amt-17-5477-2024, 2024.

1299 De Kauwe, M. G., Medlyn, B. E., Zaehle, S., Walker, A. P., Dietze, M. C., Hickler, T., Jain, A.
1300 K., Luo, Y., Parton, W. J., and Prentice, I. C.: Forest water use and water use efficiency at

https://doi.org/10.5194/egusphere-2026-3119
Preprint. Discussion started: 16 June 2026

elevated CO2: A model-data intercomparison at two contrasting temperate forest FACE sites, Glob. Chang. Biol., 19, 1759–1779, 2013.

Kidston, J., Brümmer, C., Black, T. A., Morgenstern, K., Nesic, Z., McCaughey, J. H., and Barr, A. G.: Energy balance closure using eddy covariance above two different land surfaces and implications for CO2 flux measurements, Boundary. Layer. Meteorol., 136, 193–218, https://doi.org/10.1007/s10546-010-9507-y, 2010.

Kljun, N., Calanca, P., Rotach, M. W., and Schmid, H. P.: A simple parameterisation for flux footprint predictions, Boundary. Layer. Meteorol., 112, 503–523, 2004.

Knorr, W. and Heimann, M.: Impact of drought stress and other factors on seasonal land biosphere CO2 exchange studied through an atmospheric tracer transport model, Tellus B, 47, 471–489, 1995.

Koster, R. D. and Suarez, M. J.: Energy and water balance calculations in the Mosaic LSM, National Aeronautics and Space Administration, Goddard Space Flight Center …, 1996.

Kottek, M., Grieser, J., Beck, C., Rudolf, B., and Rubel, F.: World map of the Köppen-Geiger climate classification updated, Meteorologische Zeitschrift, 15, 259–263, https://doi.org/10.1127/0941-2948/2006/0130, 2006.

Li, F., Liang, J., Kang, S., and Zhang, J.: Benefits of alternate partial root-zone irrigation on growth, water and nitrogen use efficiencies modified by fertilization and soil water status in maize, Plant Soil, 295, 279–291, https://doi.org/10.1007/s11104-007-9283-8, 2007.

Liang, X., Lettenmaier, D. P., Wood, E. F., and Burges, S. J.: A simple hydrologically based model of land surface water and energy fluxes for general circulation models, Journal of Geophysical Research: Atmospheres, 99, 14415–14428, https://doi.org/https://doi.org/10.1029/94JD00483, 1994.

https://doi.org/10.5194/egusphere-2026-3119
Preprint. Discussion started: 16 June 2026

1324 Lobell, D. B., Bänziger, M., Magorokosho, C., and Vivek, B.: Nonlinear heat effects on African
1325 maize as evidenced by historical yield trials, Nat. Clim. Chang., 1, 42–45, 2011.

1326 Martí, B., Groh, J., Canut, G., and Boone, A.: Implementation of a dry surface layer soil
1327 resistance in two, 1991–2021, 2026.

1328 Masson, V., Le Moigne, P., Martin, E., Faroux, S., Alias, A., Alkama, R., Belamari, S., Barbu,
1329 A., Boone, A., and Bouyssel, F.: The SURFEXv7. 2 land and ocean surface platform for
1330 coupled or offline simulation of earth surface variables and fluxes, Geosci. Model Dev., 6,
1331 929–960, 2013.

1332 Medlyn, B. E., Duursma, R. A., Eamus, D., Ellsworth, D. S., Prentice, I. C., Barton, C. V. M.,
1333 Crous, K. Y., De Angelis, P., Freeman, M., and Wingate, L.: Reconciling the optimal and
1334 empirical approaches to modelling stomatal conductance, Glob. Chang. Biol., 17, 2134–
1335 2144, 2011.

1336 Medrano, H., Tomás, M., Martorell, S., Flexas, J., Hernández, E., Rosselló, J., Pou, A.,
1337 Escalona, J. M., and Bota, J.: From leaf to whole-plant water use efficiency (WUE) in
1338 complex canopies: Limitations of leaf WUE as a selection target, Crop Journal, 3, 220–228,
1339 https://doi.org/10.1016/j.cj.2015.04.002, 2015.

1340 Moharana, S., Chintala, S., and Kambhammettu, B. P.: Modeling leaf and crop water use
1341 efficiency of rainfed Cotton: Interplay of environmental and biophysical drivers, Agric.
1342 Water Manag., 317, 109626, https://doi.org/10.1016/j.agwat.2025.109626, 2025.

1343 Moigne, P. L. and Boone, A.: Surfex scientific documentation, Scientific Documentation
1344 SURFEX v7, 2012.

1345 Nelson, J. A., Pérez-Priego, O., Zhou, S., Poyatos, R., Zhang, Y., Blanken, P. D., Gimeno, T.
1346 E., Wohlfahrt, G., Desai, A. R., and Gioli, B.: Ecosystem transpiration and evaporation:

https://doi.org/10.5194/egusphere-2026-3119
Preprint. Discussion started: 16 June 2026

Insights from three water flux partitioning methods across FLUXNET sites, Glob. Chang. Biol., 26, 6916–6930, 2020.

Noilhan, J. and Planton, S.: A simple parameterization of land surface processes for meteorological models, Mon. Weather Rev., 117, 536–549, 1989.

Papale, D. and Valentini, R.: A new assessment of European forests carbon exchanges by eddy fluxes and artificial neural network spatialization, Glob. Chang. Biol., 9, 525–535, 2003.

Pastorello, G., Trotta, C., Canfora, E., Chu, H., Christianson, D., Cheah, Y.-W., Poindexter, C., Chen, J., Elbashandy, A., Humphrey, M., Isaac, P., Polidori, D., Reichstein, M., Ribeca, A., van Ingen, C., Vuichard, N., Zhang, L., Amiro, B., Ammann, C., Arain, M. A., Ardö, J., Arkebauer, T., Arndt, S. K., Arriga, N., Aubinet, M., Aurela, M., Baldocchi, D., Barr, A., Beamesderfer, E., Marchesini, L. B., Bergeron, O., Beringer, J., Bernhofer, C., Berveiller, D., Billesbach, D., Black, T. A., Blanken, P. D., Bohrer, G., Boike, J., Bolstad, P. V, Bonal, D., Bonnefond, J.-M., Bowling, D. R., Bracho, R., Brodeur, J., Brümmer, C., Buchmann, N., Burban, B., Burns, S. P., Buysse, P., Cale, P., Cavagna, M., Cellier, P., Chen, S., Chini, I., Christensen, T. R., Cleverly, J., Collalti, A., Consalvo, C., Cook, B. D., Cook, D., Coursolle, C., Cremonese, E., Curtis, P. S., D'Andrea, E., da Rocha, H., Dai, X., Davis, K. J., Cinti, B. De, Grandcourt, A. de, Ligne, A. De, De Oliveira, R. C., Delpierre, N., Desai, A. R., Di Bella, C. M., Tommasi, P. di, Dolman, H., Domingo, F., Dong, G., Dore, S., Duce, P., Dufrêne, E., Dunn, A., Dušek, J., Eamus, D., Eichelmann, U., ElKhidir, H. A. M., Eugster, W., Ewenz, C. M., Ewers, B., Famulari, D., Fares, S., Feigenwinter, I., Feitz, A., Fensholt, R., Filippa, G., Fischer, M., Frank, J., Galvagno, M., et al.: The FLUXNET2015 dataset and the ONEFlux processing pipeline for eddy covariance data, Sci. Data, 7, 225, https://doi.org/10.1038/s41597-020-0534-3, 2020.

https://doi.org/10.5194/egusphere-2026-3119
Preprint. Discussion started: 16 June 2026

1370 Pique, G., Fieuzal, R., Al Bitar, A., Veloso, A., Tallec, T., Brut, A., Ferlicoq, M., Zawilski, B.,
1371 Dejoux, J.-F., and Gibrin, H.: Estimation of daily CO2 fluxes and of the components of the
1372 carbon budget for winter wheat by the assimilation of Sentinel 2-like remote sensing data
1373 into a crop model, Geoderma, 376, 114428, 2020.

1374 Potter, C., Klooster, S., Myneni, R., Genovese, V., Tan, P.-N., and Kumar, V.: Continental-scale
1375 comparisons of terrestrial carbon sinks estimated from satellite data and ecosystem
1376 modeling 1982–1998, Glob. Planet. Change, 39, 201–213, 2003.

1377 Reavis, C. W., Reba, M. L., and Runkle, B. R. K.: The effects of alternate wetting and drying
1378 irrigation on water use efficiency in Mid-South rice, Agric. For. Meteorol., 353, 110069,
1379 https://doi.org/10.1016/j.agrformet.2024.110069, 2024.

1380 Reichstein, M., Falge, E., Baldocchi, D., Papale, D., Aubinet, M., Berbigier, P., Bernhofer, C.,
1381 Buchmann, N., Gilmanov, T., Granier, A., Grünwald, T., Havránková, K., Ilvesniemi, H.,
1382 Janous, D., Knohl, A., Laurila, T., Lohila, A., Loustau, D., Matteucci, G., Meyers, T.,
1383 Miglietta, F., Ourcival, J.-M., Pumpanen, J., Rambal, S., Rotenberg, E., Sanz, M., Tenhunen,
1384 J., Seufert, G., Vaccari, F., Vesala, T., Yakir, D., and Valentini, R.: On the separation of net
1385 ecosystem exchange into assimilation and ecosystem respiration: review and improved
1386 algorithm, Glob. Chang. Biol., 11, 1424–1439,
1387 https://doi.org/https://doi.org/10.1111/j.1365-2486.2005.001002.x, 2005.

1388 Reichstein, M., Bahn, M., Ciais, P., Frank, D., Mahecha, M. D., Seneviratne, S. I., Zscheischler,
1389 J., Beer, C., Buchmann, N., and Frank, D. C.: Climate extremes and the carbon cycle,
1390 Nature, 500, 287–295, 2013.

1391 Rivalland, V., Calvet, J.-C., Berbigier, P., Brunet, Y., and Granier, A.: Transpiration and CO 2
1392 fluxes of a pine forest: modelling the undergrowth effect, in: Annales Geophysicae, 291–
1393 304, 2005.

https://doi.org/10.5194/egusphere-2026-3119
Preprint. Discussion started: 16 June 2026

1394 Roujean, J.: A tractable physical model of shortwave radiation interception by vegetative
1395 canopies, Journal of Geophysical Research: Atmospheres, 101, 9523–9532, 1996.

1396 Scott, R. L., Johnston, M. R., Knowles, J. F., MacBean, N., Mahmud, K., Roby, M. C., and
1397 Dannenberg, M. P.: Interannual variability of spring and summer monsoon growing season
1398 carbon exchange at a semiarid savanna over nearly two decades, Agric. For. Meteorol., 339,
1399 https://doi.org/10.1016/j.agrformet.2023.109584, 2023.

1400 Seneviratne, S. I., Corti, T., Davin, E. L., Hirschi, M., Jaeger, E. B., Lehner, I., Orlowsky, B.,
1401 and Teuling, A. J.: Investigating soil moisture–climate interactions in a changing climate: A
1402 review, Earth. Sci. Rev., 99, 125–161, 2010.

1403 Sharma, B. R., Gulati, Mohan, Gayathri, Manchanda, S., Ray, I., and Amarasinghe, U.: Water
1404 Productivity Mapping of Major Indian Crops, NABARD and ICRIER, 4, 88–100, 2018.

1405 Stoy, P. C., El-Madany, T. S., Fisher, J. B., Gentine, P., Gerken, T., Good, S. P., Klosterhalfen,
1406 A., Liu, S., Miralles, D. G., Perez-Priego, O., Rigden, A. J., Skaggs, T. H., Wohlfahrt, G.,
1407 Anderson, R. G., Coenders-Gerrits, A. M. J., Jung, M., Maes, W. H., Mammarella, I.,
1408 Mauder, M., Migliavacca, M., Nelson, J. A., Poyatos, R., Reichstein, M., Scott, R. L., and
1409 Wolf, S.: Reviews and syntheses: Turning the challenges of partitioning ecosystem
1410 evaporation and transpiration into opportunities, Biogeosciences, 16, 3747–3775,
1411 https://doi.org/10.5194/bg-16-3747-2019, 2019.

1412 Suyker, A. E. and Verma, S. B.: Evapotranspiration of irrigated and rainfed maize–soybean
1413 cropping systems, Agric. For. Meteorol., 149, 443–452, 2009.

1414 Suyker, A. E. and Verma, S. B.: Gross primary production and ecosystem respiration of
1415 irrigated and rainfed maize–soybean cropping systems over 8 years, Agric. For. Meteorol.,
1416 165, 12–24, 2012.

https://doi.org/10.5194/egusphere-2026-3119
Preprint. Discussion started: 16 June 2026

1417 Tanumihardjo, S. A., McCulley, L., Roh, R., Lopez-Ridaura, S., Palacios-Rojas, N., and
1418 Gunaratna, N. S.: Maize agro-food systems to ensure food and nutrition security in reference
1419 to the Sustainable Development Goals, Glob. Food Sec., 25, 100327,
1420 https://doi.org/10.1016/j.gfs.2019.100327, 2020.

1421 Tardieu, F., Simonneau, T., and Parent, B.: Modelling the coordination of the controls of
1422 stomatal aperture, transpiration, leaf growth, and abscisic acid: update and extension of the
1423 Tardieu–Davies model, J. Exp. Bot., 66, 2227–2237, 2015.

1424 Trenberth, K. E.: Water Cycles and Climate Change, Global Environmental Change, Springer,
1425 Heidelberg, 2011.

1426 Vadez, V., Pilloni, R., Grondin, A., Hajjarpoor, A., Belhouchette, H., Brouziyne, Y., Chehbouni,
1427 G., Kharrou, M. H., Zitouna-Chebbi, R., and Mekki, I.: Water use efficiency across scales:
1428 from genes to landscapes, J. Exp. Bot., 74, 4770–4788, 2023.

1429 Wang-Erlandsson, L., Van Der Ent, R. J., Gordon, L. J., and Savenije, H. H. G.: Contrasting
1430 roles of interception and transpiration in the hydrological cycle - Part 1: Temporal
1431 characteristics over land, Earth System Dynamics, 5, 441–469, https://doi.org/10.5194/esd-
1432 5-441-2014, 2014.

1433 Xue, B.-L., Guo, Q., Otto, A., Xiao, J., Tao, S., and Li, L.: Global patterns, trends, and drivers
1434 of water use efficiency from 2000 to 2013, Ecosphere, 6, art174,
1435 https://doi.org/https://doi.org/10.1890/ES14-00416.1, 2015.

1436 Yang, L., Qu, H., Zhang, Y., and Li, F.: Effects of partial root-zone irrigation on physiology,
1437 fruit yield and quality and water use efficiency of tomato under different calcium levels,
1438 Agric. Water Manag., 104, 89–94, https://doi.org/10.1016/j.agwat.2011.12.001, 2012.

https://doi.org/10.5194/egusphere-2026-3119
Preprint. Discussion started: 16 June 2026

1439 Yu, G., Song, X., Wang, Q., Liu, Y., Guan, D., Yan, J., Sun, X., Zhang, L., and Wen, X.: Water-
1440 use efficiency of forest ecosystems in eastern China and its relations to climatic variables,
1441 New Phytologist, 177, 927–937, https://doi.org/10.1111/j.1469-8137.2007.02316.x, 2008.

1442 Zhou, S., Yu, B., Huang, Y., and Wang, G.: The effect of vapor pressure deficit on water use
1443 efficiency at the subdaily time scale, Geophys. Res. Lett., 41, 5005 – 5013,
1444 https://doi.org/10.1002/2014GL060741, 2014.

1445